Chemiluminescence “Add-and-Measure” Sensing Paper Based on the Prussian Blue/Metal-Organic Framework MIL-101 Nanozyme for Rapid Hydrogen Peroxide Detection

Chemiluminescence "Add-and-Measure" Sensing Paper Based on the Prussian Blue/Metal−Organic Framework MIL-101 Nanozyme for Rapid Hydrogen Peroxide Detection

Hector Martinez-Perez-Cejuela[1], Maria Maddalena Calabretta[2], and Elisa Michelini[2,3]*

[1] *Department of Analytical Chemistry, University of Valencia, 46100 Burjassot, Valencia, Spain*

[2] *Department of Chemistry "Giacomo Ciamician", University of Bologna, 40129 Bologna, Italy*

[3]*IRCCS Azienda Ospedaliero-Universitaria di Bologna, 40138 Bologna, Italy*

*Corresponding author:

Prof. Elisa Michelini

University of Bologna

Dept. of Chemistry "Giacomo Ciamician"

Via P. Gobetti 85, 40129 Bologna, Italy

elisa.michelini8@unibo.it

Abstract

In this work, a chemiluminescent sensing paper has been developed using a peroxidase biomimetic metal−organic framework as a versatile host platform. For the first time, we have explored the use of in situ growth of Prussian Blue nanoparticles (PB-NPs) onto the MIL-101(Fe) structure for the assembly of a ready-to-use sensing paper. In situ growth of PB-NPs has been performed on the surface of the MIL-101(n) family. This novel composite, named PB-NPs@MIL-101(Fe), has been successfully used to develop a sensing paper for one-step detection of H_2O_2 in real samples (commercial disinfectant solutions and tap water samples). The as-prepared material was fully characterized, including X-ray analysis, Fourier transform infrared, scanning and transmission electron microscopies, nitrogen isotherms, and elemental analysis. After the characterization, the analytical performance of the PB-NPs@MIL-101(Fe) sensing paper was evaluated. The low-cost sensor (0.15 euro per unit) was able to detect down to 8.2 μM (corresponding to 8.2×10^{-11} mol) H_2O_2 using only 10 μL of sample with satisfactory reproducibility (relative standard deviation 17%).

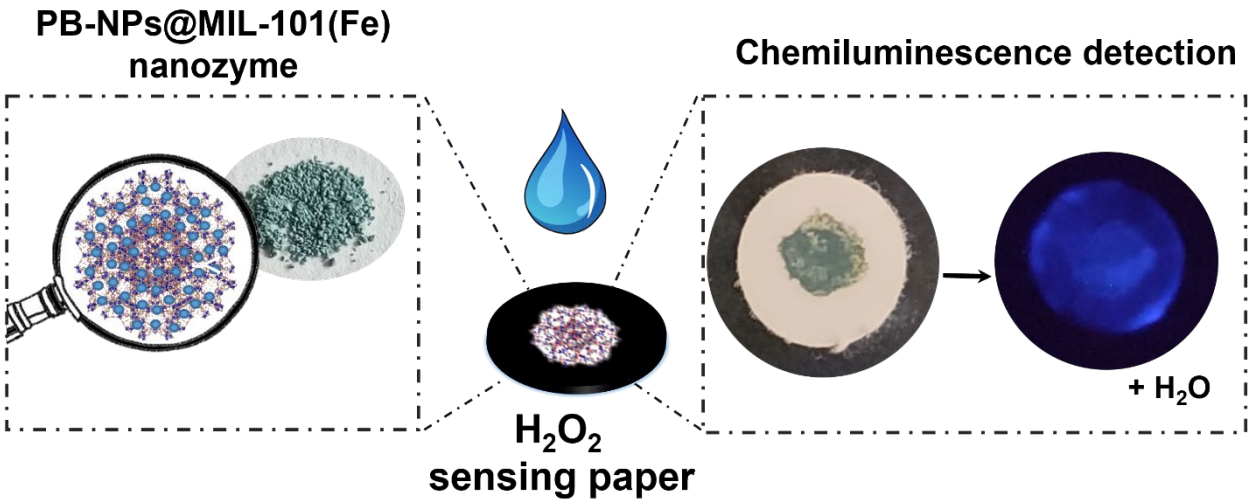

1. Introduction

The analysis and accurate determination of hydrogen peroxide (H_2O_2) is of significant concern since this analyte is employed in several industrial fields and is widely found in water, food, and air. Moreover, it is also a secondary product of cell metabolism connected to oxidative stress.[1,2] For this reason, H_2O_2 is also a marker of several diseases, for example, its increase in breath condensate has been correlated to asthma, cystic fibrosis, and other pulmonary diseases.[3] In addition to its applications in medicine, hydrogen peroxide is a key component in many commercial disinfectants and industrial formulations, requiring precise monitoring to ensure efficacy and safety. Laboratory-based analytical methods relying on luminescence and titrimetric approaches are generally employed for H_2O_2 analysis. However, their practical use is limited by a lack of portability, the use of large amounts of solvents/reagents, high costs, and the need for skilled personnel. Sensor-based methods have also been proposed in the past decade.[4,5] These approaches are mainly based on enzymes able to reduce H_2O_2, leading to the production of chromogenic, fluorescent, or chemiluminescent (CL) products. In this context, horseradish peroxidase, a 44 kDa glycoprotein that catalyzes the reaction of hydrogen peroxide with electron-donating substrates, has been commonly used as a model enzyme, being its main limitation the scarce stability in nonphysiological conditions[1] as well as the cost-effectiveness. As an alternative, the use of catalytic nanomaterials (nanozymes) that mimic enzymes has several advantages, such as strong activity, ease of synthesis, affordability, and stability. Several nanozymes have been reported based on metallic centers, magnetic nanoparticles (Fe_3O_4), carbon nanotubes (CNTs), Prussian Blue nanoparticles (PB-NPs), and metal−organic frameworks (MOFs).[1,6]

PB is a mixed-valent iron(III) hexacyanoferrate compound with interesting redox behavior,[7] which can help reduce H_2O_2 catalytically with a high rate and low overpotential without interference reduction of coexisting substances.[8,9] Both properties are related to the zeolite-like structure of PB that favors the penetration of small molecules; meanwhile, larger molecules (such as glucose, uric/ascorbic acid, etc.) are excluded.[10] Despite these appealing features, the direct use of PB-NPs for the obtainment of H_2O_2 sensors is somehow hindered by some aspects: (i) during the reduction, PB-NPs could be destroyed due to the weakness of the Fe(III)−N bond;[11] (ii) the blue-color interference with colorimetric detection; and (iii) low stability in aqueous medium with the formation of aggregates affecting the catalytic properties.[12] On the other hand, MOFs are interesting functional materials composed of the coordination of organic ligands and metal centers.[13] The rise of their popularity in recent years is due to their advantageous properties such as high porosity, tunable surface, large surface area, and thermal/chemical robustness.[14] As a result, MOFs have been widely applied in many different fields, including energy storage, bioimaging, separation, sample treatment, and catalysis.[15] Some MOF structures have shown efficient peroxidase-like catalytic activity by themselves, and, thanks to their superior stability and low cost, they can be used as alternatives to enzymes for sensing and catalysis applications.[16] The synthesis of PB-NPs@MOF composites and their application in the sensing field has been recently explored elsewhere[17,18] as well as the implementation of PB-NP into cellulose sensors.[19] Both have shown peroxidase mimic properties; however, their fruitful combination with enhanced properties has not yet been reported for chemiluminescence add-and-measure paper sensing. In this context, we have proposed a novel concept of a paper sensing platform by the in situ growth of PB-NPs onto the surface of MIL-101(Fe) for use as an artificial enzyme peroxidase. To the best of our knowledge, this is the first report exploiting the synergistic effect of both MOF and

PBNPs for the design of a CL paper-based sensing platform. This approach could represent a feasible alternative to traditional H_2O_2 detection methods, with the advantages of high throughput, greenness, reduced consumption of reagents, and low cost. Several MOFs from the MIL-101 family were studied, including those containing Fe, Al, and Cr as metal centers. Furthermore, the importance of the presence of MOF was evaluated by the comparison of the results with bare PB-NPs. The paper-based platform was optimized regarding the reagent concentrations and sample volumes. The composite was also chemically and morphologically characterized to confirm its successful synthesis and to better understand the results. The selection of paper as a support was also exploited to provide a user-friendly platform that can be easily produced with an office wax printer. A limit of detection (LOD) as low as 8.2 μM (corresponding to 8.2×10^{-11} moles) and a Michaelis− Menten constant (Km) of 382 ± 17 μM (corresponding to 3.82×10^{-9} moles) were obtained. Moreover, the paper sensor had a storage stability of at least 2 weeks at room temperature (28 °C). Prompted by the encouraging results obtained, we successfully demonstrated the applicability of this sensing platform by applying this method to real samples with good analytical performance. The ability to detect H_2O_2 in these real-world matrices highlights the practical significance of our sensor. By demonstrating compatibility with commercial formulations, this work establishes the sensor's potential for widespread industrial and consumer use.

2. Experimental Section

Reagents and Materials. Aluminum chloride hexahydrate, chromium(III) nitrate nonahydrate, iron chloride(III) hexahydrate, terephthalic acid (TA), $K_4[Fe(CN)_6]\cdot 3H_2O$, sodium alginate, polyvinylpyrrolidone (Mw 1000), hydrogen peroxide, Trizma hydrochloride, and citric acid were obtained from Merck KGaA (Darmstadt, Germany). Solvents (e.g., dimethylformamide (DMF), hexane, methanol, and others) were of high-

performance liquid chromatography grade and were provided by VWR International Eurolab (Milan, Italy). SuperSignal ELISA Femto Maximum Sensitivity Substrate was obtained from Thermo Scientific (Waltham, MA, USA). Chromatographic CHR cellulose paper, Whatman number 1 (W1), was acquired from GE Healthcare (Chicago, IL, USA), and the hydrophobic barriers were obtained by wax printing (Xerox, Norwalk, CT, USA). Milli-Q (MQ) water was purified by the Rephile Bioscience Millipore system. All other reagents used were of analytical grade unless otherwise stated. Instrumentation. A desktop wax printer (ColorQube 8570, Xerox) was used to modify the surface of the W1 paper. Varioskan LUX (Thermo Scientific, Waltham, MA, USA) equipped with automatic injection was used to perform the CL studies. Scanning electron microscopy (SEM) images were obtained with a Hitachi S-4800 microscope (Ibaraki, Japan) coupled to a retro dispersive electron detector and another energy dispersive detector (EDAX Genesis 40). Transmission electron microscopy (TEM) images were acquired with a JEM1010 JEOL microscope coupled to an AMT RX80 digital camera (Akishima, Japan). Analysis by powder X-ray diffraction (p-XRD) analysis was carried out using a diffractometer model D8 ADVANCE A25 (Bruker, Hamburg, Germany). Attenuated total reflection Fourier transform infrared (FT-IR) was recorded on a Bruker FT-IR spectrometer (Bremen, Germany) model Tensor 27 using a DuraSamplIR II accessory and a 9-reflection diamond/ZnSe DuraDisk plate (Smiths Detection Inc., Warrington, UK). Adsorption−desorption N2 isotherms were assessed with the S5Micromeritics ASAP2020 instrument (Norcross, USA) at 77 K. The specific surface area and porosimetry characteristics were obtained by applying the Brauner−Emmet−Teller (BET) and Barrett−Joyner−Halenda mathematic models, respectively.

Synthesis of MIL-101(Fe). The syntheses of bare PB-NPs and other MOFs containing Cr and Al are described in detail in the Supporting Information. MIL-101(Fe) was

synthesized according to our previous report with some modifications.[20] Briefly, iron(III) chloride hexahydrate (5 mmol) and TA (2.5 mmol) were weighed and dissolved in DMF (15 mL). The molar ratio was fixed at 1:2:194 for TA/Fe(III)/DMF. The mixture was homogenized by vortexing (5 min), followed by an ultrasonic bath (10 min). A Teflon-lined stainless-steel autoclave was used to seal the mixture and to perform the solvothermal reaction for 24 h at 110 °C. Then, the reaction container was cooled to room temperature. The resulting dark brown material was collected by centrifugation at 14,000g for 10 min and washed with DMF (3 × 10 mL) to remove the unreacted MOF precursors. The as-synthesized MIL-101(Fe) was further purified with methanol at 60 °C for 2 h to exchange the solvent. The activated material was centrifuged at 14,000g for 10 min and dried at 80 °C for 8 h.

Synthesis of PB-NPs@MIL-101 (Fe). The in situ growth of PB-NPs on the MIL-101 (Fe) surface was carried out following a previously reported procedure with some modifications.[17] Briefly, 100 mg of dehydrated MIL-101 (Fe) was suspended in 50 mL of n-hexane (hydrophobic solvent) for 15 min in an ultrasonic bath and vortexed every 5 min. Afterward, 2 mL of 100 mM aqueous $K_4[Fe(CN)_6]\cdot 3H_2O$ (hydrophilic solvent) was added dropwise for 10 min under vigorous stirring. At this point, the MOF was moved from the hexane to the aqueous solution, forming colored drops. Slight visual changes were observed in MOF containing Cr or Al metals to a bluish color, and in the case of Fe-MOF, a change from brown to dark blue was observed, indicating the immediate formation of a remarkable amount of PB-NPs onto the surface within the first step (Figure 1). The reaction was kept under stirring for 2 h under atmospheric conditions. Then, the organic solvent was discarded by decanting, and the aqueous fraction was washed four times with 50 mL of ddH_2O. The first two washing fractions were blue, indicating the removal of nonattached PB-NPs. The resulting solids were dried at 50 °C for 2 h, and

then the temperature was increased to 100 °C for 8 h. In a second step, the dried material ([Fe(CN)$_6$]$_4$@MIL-101(Fe)) used as seed for the growth of PB-NPs, presumably via electrostatic interactions,[21] as mixed with 50 mL of n-hexane and dispersed for 15 min in the ultrasonic bath, vortexing every 5 min. Then, 2 mL of 100 mM aqueous FeCl3 solution was added dropwise for 20 min under vigorous stirring, and the reaction was kept for 2 h. After stirring, the precipitated solid was washed and dried, and the resulting blue MOF (Figure 1) was washed and dried, as described before.

Fabrication of the PB-NPs@MIL-101 (Fe) Paper Sensor. To fabricate the paper sensor platform, wax printing was used to create hydrophobic zones in the W1 Chromatographic CHR cellulose paper. Circular 5.0 mm diameter wells were designed with PowerPoint (Microsoft, Redmond, WA, USA). The paper was heated at 100 °C for 1 min to melt the deposited wax. Then, individual units were cut (size 0.3 × 0.3 cm) and introduced into the black 96-well plate. A 15 µL volume of commercial luminol (SuperSignal ELISA Femto Maximum Sensitivity Substrate) was deposited on the hydrophilic zone and dried at 60 °C for 45 min. In the meantime, an aqueous dispersion was prepared containing 500 mg $^{L-1}$ of PB-NPs@MIL-101(Fe) and 1% (m/v) of sodium alginate in 50 mM Tris−HCl pH 7.8. After complete evaporation of luminol solution, 10 µL of the MOF-based fadispersion was added, and the solution was evaporated at 60 °C for 20 min. After this process, sensing papers were stored at room temperature until use (Figure 1).

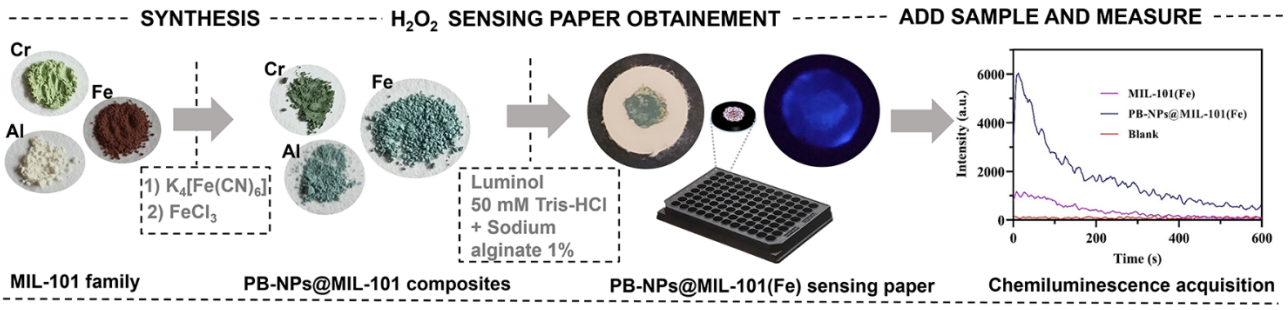

Figure 1. Schematic representation of the workflow for obtainment of the biomimetic peroxidase sensing paper and representative image acquired with a OnePlus 6T smartphone

CL Paper Sensor Characterization and Method Development. The kinetic emission of PB-NPs@MIL101(Fe) was characterized with a benchtop luminometer. The acquisition of the CL signal (10 min, 0.5 s integration time) was performed in a black 96-well plate (Greiner Bio One North America, Monroe, NC, USA) after automatic injection of H_2O_2. All of the experiments were carried out in triplicate and repeated at least three times to remove potential outliers. Data treatment was performed with Microsoft Excel (Microsoft Office, WA, USA) and GraphPad Prism v.8 software (GraphPad Software, La Jolla, USA). The following parameters were analyzed: precision, accuracy in commercial H_2O_2 samples, Km, LOD, LOQ, and storage stability (at 4 and 28 °C). For instance, the precision was evaluated by the calculation of relative standard deviation (RSD) (%) between intrabatch (same material synthesis, same day) and interbatch (different material synthesis, different days) analyses. The accuracy was assessed by the analysis of commercial H_2O_2 pharmaceutical products (declared content 3.0%). Dose− response curves were obtained for H_2O_2 samples ranging from 0.001 to 5.0 mM for LOD and LOQ determination (calculated as blank plus 3 or 10 times the standard deviation of the CL signal of four replicates of a blank solution, respectively) and Km for H_2O_2. In optimized conditions, the H_2O_2 sensing paper requires only 10 μL of sample, and measurements are performed at room temperature without requiring any incubation time.

H_2O_2 Quantification in Real Samples and Stability. The suitability of the developed paper-based platform was investigated by analyzing real samples, including tap water samples and commercial H_2O_2 solutions. Tap water samples were spiked with low and

medium concentrations of H_2O_2 (0.002 and 0.01 mM). All analyses were performed 6 times to remove potential outliers. For sensor stability studies, four ready-to-use paper platforms were synthesized the same day (t0) and were kept at 4 and 28 °C in the darkness for 2 weeks. The CL signal was acquired at different time points according to the optimized protocol and compared with freshly made sensors. Stability studies at different pH values were performed by analyzing H_2O_2 (0.1 mM) with the PB-NPs@MIL-101(Fe) sensing paper in 50 mM Tris−HCl by adjusting the pH to 5.0, 7.4, and 10.0, respectively.

3. Result and Discussion

The use of new materials with the ability of artificial enzyme mimetics is a topic of outstanding interest in the scientific community. The combination of MOF and paper sensing to obtain functionalized paper-based sensors showed significant improvements in analytical performance and stability.[22] A family of MIL-101 nanomaterials was selected based on previous studies[12,17] to develop a paper sensor for H_2O_2 detection. The selection of MIL-101 and PB-BPs to address the requirements of a paper-based analytical platform derives from different factors. First, both materials possess intrinsic peroxidase−mimic activity;[23] second, the PB-NP dispersibility is low with a high tendency to form aggregates in water over time. Therefore, PB-NPs direct deposition on a paper support to obtain a ready-to-use sensor would not be not feasible. On the contrary, by combining both materials, the sensor can be easily prepared in any laboratory without specialized or sophisticate instrumentation (Figures S1 and S2). The MIL101 family is characterized by a high surface area, a zeotype crystal structure with an internal pore diameter of around 32 Å, and pore windows of 12−16 Å, increasing analyte-MOF interaction.[24] Different PB-NPs@MIL-101 were fabricated, including Cr, Al, and Fe as metal centers. The decoration of the MOF surface with PB-NPs into host materials was performed via a one-pot approach, using mild conditions. To select the best PB-NPs@MIL-101 as biomimetic

peroxide, a batch experiment using a 384-well plate was performed. In so doing, a 5.0 μL volume of the synthesized PB-NPs@MIL-101 dispersions (500 mg L^{-1}) was mixed with 5.0 μL of luminol 0.025 M (pH 12.0) and 10.0 μL of 10 mM H_2O_2. As expected, significant chemiluminescence signal enhancements were observed, i.e., 1.22 and 1.61 greater, compared to those samples without MOFs when MIL-101(Cr) and MIL-101(Fe) were present, respectively. No signal enhancement was observed with Al-based MOF.[12,17] As shown in Figures 2A,B, S3, and S4, the presence of PB-NPs in the final composite is clearly evidenced in the case of Fe material; meanwhile, no characteristic peaks from PB-NPs are shown in Al or Cr materials. A possible explanation refers to the limited amount of PB-NPs on their surface, which is not sufficient to increase the signal as in MIL-101(Fe), probably due to the presence of Fe(II)/Fe(III) source onto the surface, the PB growth is favored. Prompted by these results, MIL-101 containing Fe was further investigated. In this case, the concentration of H_2O_2 was decreased 100 times to assess the behavior of PBMIL-101(Fe) in such a scenario. As shown in Figure S1, MIL101(Fe) was unable to act per se as a nanozyme, with a chemiluminescence intensity comparable to that of the blank. Conversely, the in situ growth of PB-NPs at the MIL-101(Fe) network (blue trace) increased the CL signal response drastically (ca. 10-fold), which is comparable with bare PBNPs (conc. x/10). The real applicability of the developed material was assessed in a sensing paper, consisting of 10 μL of commercial luminol and 10 μL of 2000 mg L^{-1} PB-NPs@MIL-101(Fe) (or bare MIL-101(Fe) or PB-NPs) dried 15 min at 50 °C for each one. After that, 10 μL of H_2O_2 0.1 mM was automatically injected, and the CL signal was acquired. Probably due to their instability and proneness to aggregation, especially at basic pH,[12] bare PB-NPs did not show activity, highlighting the stability under both atmospheric and aqueous conditions of the PB-NPs@MIL-101(Fe) in the sensor design compared to bare MIL-101(Fe) and PB-NPs (Figure S2).

The catalytic mechanism of PB-NPs@MIL-101(Fe) in colorimetric detection has been studied,[17] confirming that of other MOF structures.[25,26] Briefly, the decomposition of H_2O_2 into O_2 is favored near the MOF network via electron transfer by a Fenton-like reaction, which increases the generation of radicals (e.g., • OH or • O2−) that react with luminol, forming luminol radicals. These products are responsible for reacting with monodissociated hydrogen peroxide, giving rise to light emission proportional to the H_2O_2 concentration. Besides, MIL-101(Fe) already presents in the MOF network vacant Fe^{3+} sites, which favor the in situ growth of higher content of PB-NPs.

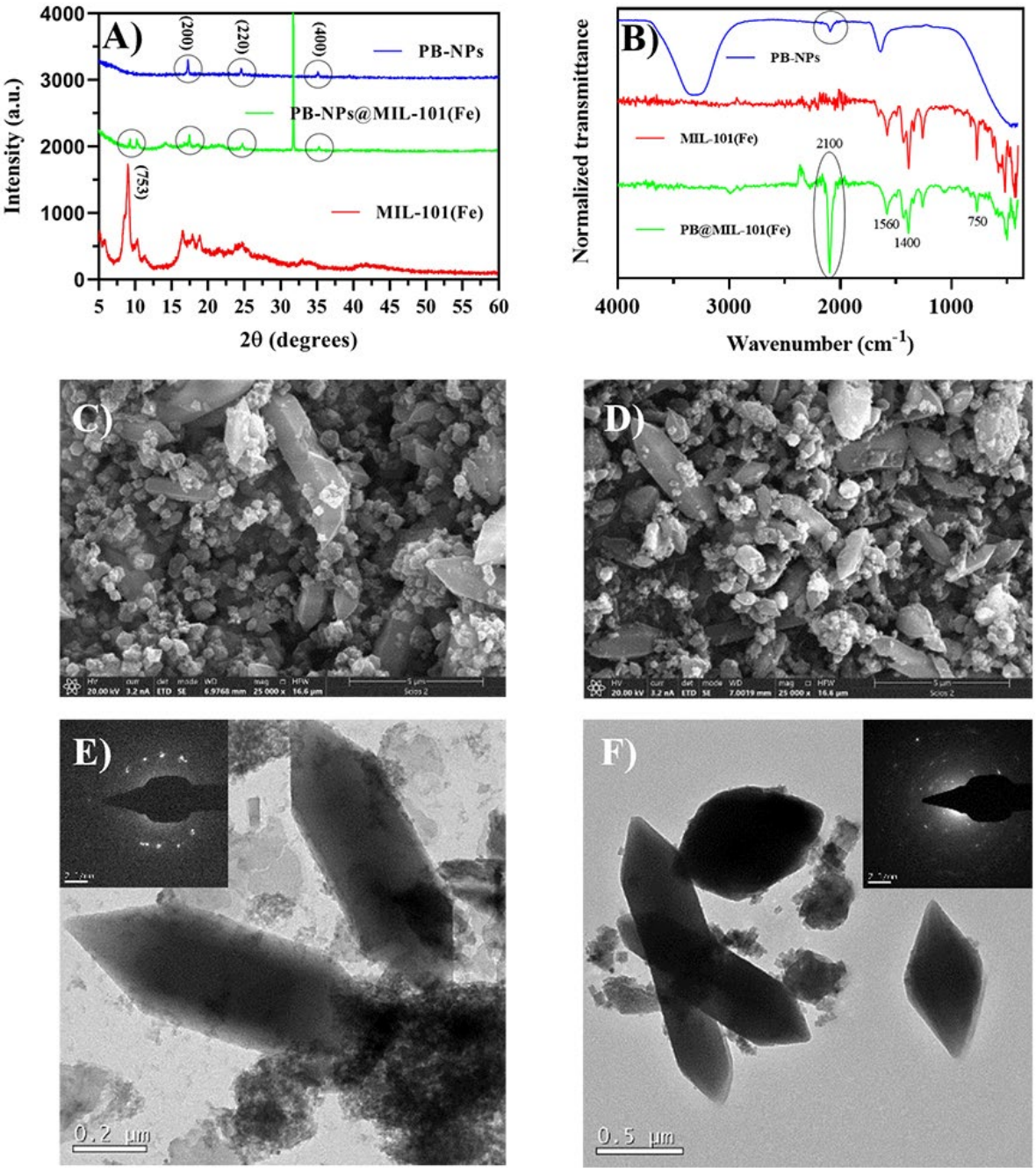

Figure 2. Characterization studies from MIL-101(Fe). (A) p-XRD from the PB-NPs, MIL-101(Fe), and PB-NPs@MIL-101(Fe); (B) FT-IR from the composite, paper, and PB-MOF@paper; (C,D) SEM images at ×25k of magnification from MIL-101(Fe) before and after the PB-NPs growth, respectively; (E,F) TEM images from MIL101(Fe) before and after the PB-NPs growth, respectively.

The presence of PB can increase the electron transformation between catalysts and substrates, whereas the presence of MIL-101(Fe) will contribute to the expansion of the pore space,[21] enabling H_2O_2 to diffuse into the pores and resulting into production of more active radical species, like $^{\bullet}OH$ and $O^{2\bullet-}$, thus enhancing light emission. Therefore, the material was selected as a candidate for developing an "add-and-measure" sensing paper for H_2O_2 in which luminol is oxidized without adding other oxidants.

Characterization of PB-NPs@MIL-101(Fe). Once PBNPs@MIL-101(Fe) was selected as the best candidate, the material was characterized in depth by several techniques. Furthermore, the other candidates were also evaluated to corroborate their correct synthesis, as well as to support the analytical results. For instance, the crystallinities and corresponding diffraction patterns were checked with p-XRD. Figure 2A shows the pattern of MIL-101(Fe) before and after the in situ growth of PB-NPs. The MIL-101(Fe) patterns fit with other works reported in the literature.[27,28] Interestingly, the typical diffraction spectra (red trace) disappeared after the postsynthetic modification, in which the PB-NPs pattern is present (trace green and blue). This result suggests that the covering of MIL-101(Fe) by PB-NPs may be fully achieved, and only that characteristic pattern (200, 220, and 400) can be distinguished,[29] together with the double peak around 8° (753) from MIL-101(Fe). This trend was not observed in the case of MIL-101(Cr and Al), which could be attributed to the lower proportion of PB-NPs on the surface (Figure S3). On the other hand, FT-IR was also evaluated (Figures 2B and S4). The typical band centered at 2100 cm^{-1}, attributed to the Fe^{3+}−N≡C−Fe^{2+} vibration,[30] is present in both PB-NPs and PB-NPs@MIL-101(Fe); meanwhile, this peak is very small for the other metals. MIL-101(Fe) presented the typical peaks around 1560, 1400, and 750 cm^{-1} , which matched with C−H and COO, respectively, indicating the presence of the organic ligand (BDC linker) in the MIL-101(Fe) structure.31 The low relative intensity of the 2100 cm−1 peak

(C≡N stretch from PB-NPs) in the aqueous solution is due to normalization by the strong OH peak at 3200 cm^{-1}. In contrast, the powder format of PB@MIL-101(Fe) shows a relatively intense 2100 cm^{-1} peak as no strong peak normalizes the spectrum, and PBNPs almost fully cover the MOF surface and pores (as observed in N_2 isotherm studies). In addition, the sensing paper was evaluated by FT-IR spectroscopy (Figure S5). It must be noted that the proportion of the composite compared to the paper matrix is relatively low, thus decreasing the characteristic peak intensities from MOF. The morphologies were examined by SEM and TEM microscopies. The structure of MIL-101(Fe) can be observed in Figure 2C, and the typical polyhydric shapes are depicted.[32,33] It is worth mentioning that, after the PB growth, the morphology did not change (Figure 2D), which implies that the synthesis conditions were not harmful to the bare MOF. Furthermore, the dispersion of iron has been verified with EDX and mapping analysis, which indicated that the amount of Fe increased from 1.7 to 4.1 wt % (Figure S6). The other material micrographs, including bare MOFs and their corresponding composites, are shown in Figure S7. TEM images were also performed (Figure 2E,F), showing some differences before and after PB-NP growth thanks to the measure of transmitted electrons and the higher resolution. Although the morphology did not change, darker tonalities are visible in PB-NPs@MIL-101(Fe), probably due to the homogeneous covering of the surface. TEM images for the other metal materials are shown in Figure S8. Besides, the adsorption/desorption nitrogen isotherms were acquired not only to obtain the porosity but also to study the influence of PB-NPs growth on the surface area. Typical type IV isotherms were obtained for all materials, which is normal for a MOF structure containing mesopores (from MOF aggregation) and micropores (internal cavities). The surface areas for the bare MIL-101 (Fe, Cr, and Al) were calculated by applying the BET approach with resulting values of 1890, 1530, and 1250 $m^2\ g^{-1}$, respectively. Surprisingly, after the PB-NPs synthesis, the

area was drastically reduced by about >95% in all cases, which suggests that all the pores were completely fulfilled homogeneously with the PB-NPs (Figure S9).[12]

Method Optimization. To improve the analytical performance and to identify the best compromise between the enhanced CL signal and reduced volume of reagents, several parameters were optimized, such as the volume of luminol solution (5, 10, and 15 μL), the MOF amount (from 2.5 to 10 μg), the volume of sample/H_2O_2 standard (from 10 to 20 μL), and the presence of additives (Figure 3). In the optimized conditions, 15 μL of luminol, 5 μg of MOF-based composite, 10 μL of sample, and the addition of sodium alginate (1% m/v as dispersant agent) were added on paper. The first approach for the design and assembly of the sensing paper was based on previous studies using wax printing.[34,35] Circular reaction zones with 5 mm of diameter were produced, and the CL signal obtained with 15 μL of luminol was 4 and 8 times higher than that obtained using 10 and 5 μL, respectively (Figure 3A), probably due to the favored reaction process in the presence of luminol excess as well as the higher amount of enhancers/stabilizers. Then, the PB-NPs@MIL-101(Fe) amount was varied, including amounts from 2.5 to 10.0 μg using 10.0 μL of dispersions with concentrations ranging between 250 and 1000 mg L^{-1} (Figure 3B). The presence of 2.5 μg PB-NPs@MIL-101(Fe) produced a lower CL signal than that obtained with 5.0 μg, probably due to the reduced catalytic activity (35%) with less material (1/2). However, when the amount of the MOF-based composite was increased twice, the signal reduced by about 25%. The explanation of this result is not trivial, and it could arise from the aggregation of MOF particles forming clusters, which hinder their dispersion in solution. This fact can also support the high imprecision when a high amount of MOF is used since the covering of the sensor is not completely homogeneous. For this reason, 5.0 μg of PB-NPs@MIL-101(Fe) was fixed as the optimum amount for the sensor manufacturing. Next, the use of additives in the MOF

dispersion was also studied to achieve homogeneous solutions (Figure 3C). In this sense, PVP (Mw 1000)[36] and sodium alginate[37] were tested. The results suggest that the use of any of both has increased the CL response by around 44− 50%, perhaps for better dispersibility of the MOF (Figure S10), especially when sodium alginate is used. Hence, the selection of sodium alginate was mainly based on the ability to maintain the MOF dispersed for long periods as well as the slight enhancement in the signal response with respect to PVP (∼10%). The effect of sample volume was also assessed using volumes from 10.0 to 20.0 μL of a 0.1 mM H_2O_2 standard solution (Figure 3D). As depicted, no significant differences were achieved when the volume was increased from 10.0 to 15.0 μL due to the excess of analyte. However, higher volumes, such as 20.0 μL, decreased the CL intensity up to 42%, which clearly indicates that the volume that the hydrophobic barriers can support has been exceeded. Based on these results, 10.0 μL was selected as the optimal sample volume due to the lower RSD (4%) compared to that obtained with 15.0 μL (12%). In addition, the effect of pH was evaluated (Figure S11). The luminol−oxidant reaction (H_2O_2 and ($K_3[Fe(CN)_6]$) produces weak blue chemiluminescence, which increases in alkaline conditions.38 However, according to the stability of MIL101(Fe)-based materials, the optimal pH conditions should be comprised between pH 4.0 and 11.0, thus avoiding extreme conditions, which in addition could alter the sample.[39]

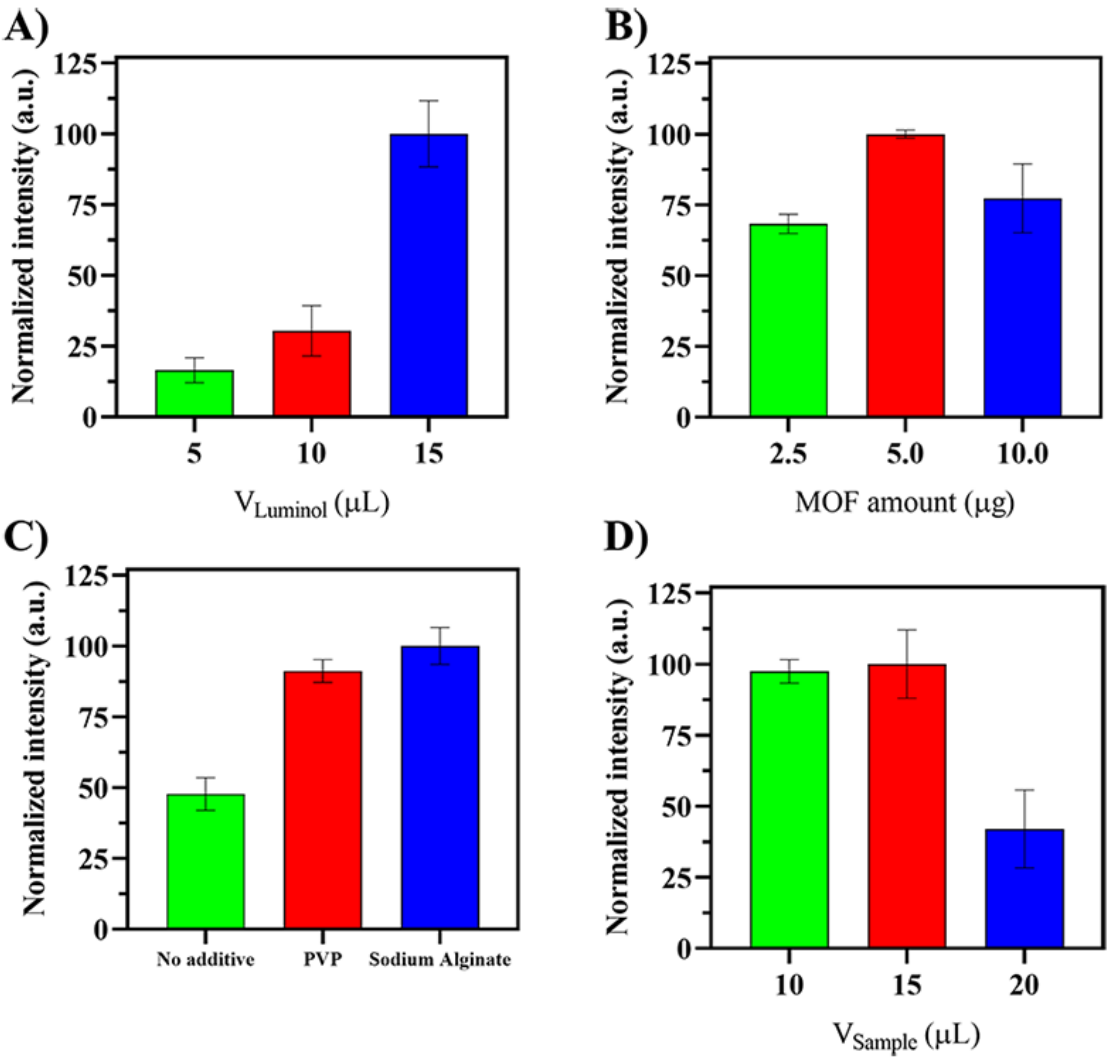

Figure 3. Optimization of the method parameters using the developed MOF@paper sensor. (A) Volume of commercial luminol solution evaporated; (B) amount of MOF deposited onto the sensor; (C) use of additives on MOF dispersion in the sensor manufacturing; (D) sample volumes injected.

Furthermore, under acidic conditions, protonation made the MIL-101(Fe) positively charged, attracting more H_2O_2 onto its surface. On the contrary, in the presence of alkaline conditions, H_2O_2 will react with OH^- to produce perhydroxyl ions (HO^{2-}), reducing the

available H_2O_2.[40] Furthermore, OH^- can be adsorbed onto the Fe(III) cluster, resulting in MIL101(Fe) inactivation.[41] Therefore, the optimal conditions were defined at pH 8.0 for further studies.

Kinetic Studies and Analytical Performance of PBNPs@MIL-101(Fe). Once the analytical procedure was optimized, some analytical parameters, such as precision, *K*m, linear range, LOD, LOQ, accuracy, and storage stability, were investigated. The former was studied using the same batch

sensor at the same time (intraday) and using different batch sensors for one month (interday), with these precision values below 17% (RSD). The results are summarized in Table 1 as the average of 6 individual measures. Furthermore, the apparent K_m was experimentally calculated in the presence of

varying concentrations of H_2O_2 (from 0.001 to 1 mM). The CL intensity was calculated from 3 independent measurements as the average of the maximum intensity. According to the Michaelis−Menten equation, the obtained value for the K_m was (382 ± 17) μM and 3.65 M s^{-1} for the V_{max}.

Table 1. Precision Studies for the Optimized PB-NPs@MIL-101(Fe) Sensor[ab]

H_2O_2 conc. (mM)	time (s)	precision (RSD, % n = 6)	
		intrabatch	interbatch
0.01	intensity maximum	3.7	5.4
	30	8.5	9.1
	60	7.2	4.6
0.10	intensity maximum	0.5	10.2
	30	1.4	8.9
	60	10.6	16.4
1.00	intensity maximum	7.0	3.4
	30	6.8	9.2
	60	5.0	15.8

[a]Intrabatch values (n = 6, in the same day) using the same MOF synthesis and reagent batch. [b]Interbatch values (n = 6, in different days) using different MOF synthesis and reagent batches.

This result indicates good accessibility for the substrate in the presence of the MOF, mainly attributed to the large surface area of the MIL-101(Fe) and the large amount of PB-NPs on the surface. The applicability of the developed sensor was also studied by calculating the linear range, the LOD and the LOQ of this method. For this purpose, H_2O_2 dose–response curves were obtained following the same procedure (Figure 4A). The LOD and LOQ values were calculated as the blank plus three or ten times the standard deviation of three independent replicates, respectively. The LOD and LOQ values were 8.2 and 19.0 μM, and a linear range from 19 to 100 μM was obtained.

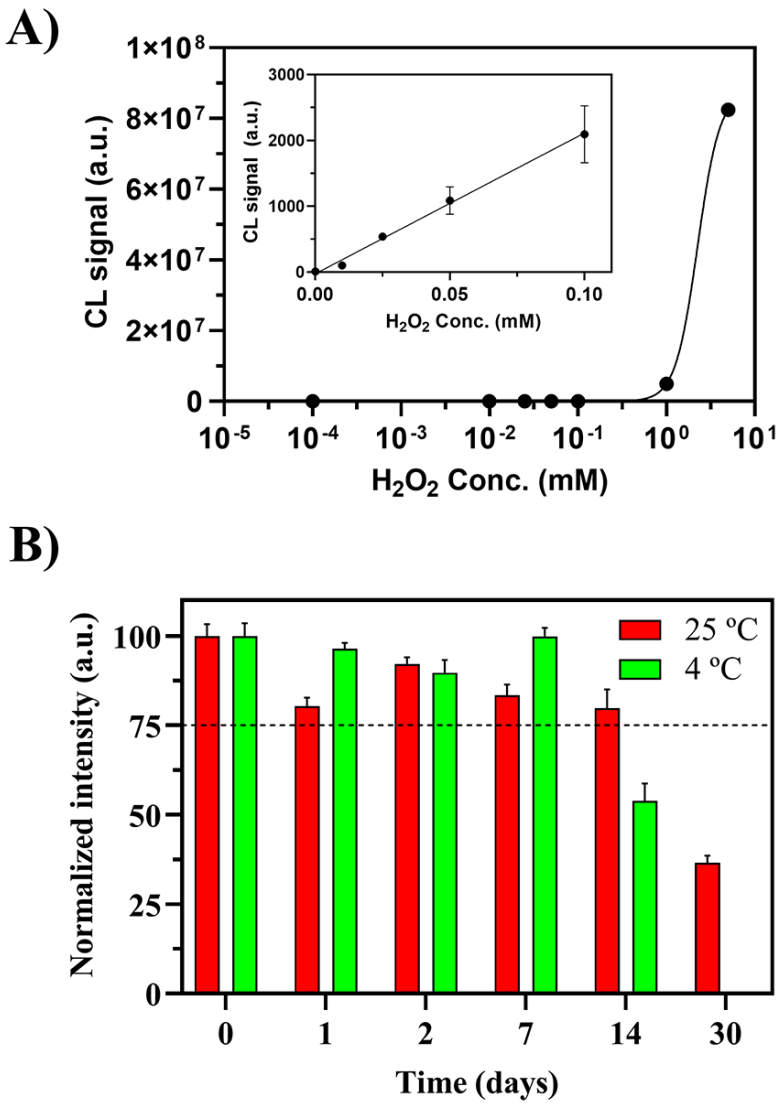

Figure 4. (A) Dose−response curve for H_2O_2. The inset represents the linear correlation in the lower range of the CL signal response vs H_2O_2 concentrations; (B) CL kinetic studies for the storage stability at different periods of time.

This is a satisfactory value considering the assay format, the very low volumes of reagents, and potential applicability also for on-site analyses with portable instrumentation. The accuracy of the method was evaluated using commercial H_2O_2 formulations bought in a local market using the optimized protocol described in the "Experimental Section". The results are shown in Table 2.

Table 2. Accuracy Studies for the Optimized PB-NPs@MIL-101(Fe) Sensor (a) Commercial Formulation and (b) Spiking at Two Different H_2O_2 Concentrations in Tap Water Samples

	expected conc. (mM)	found (mM)	accuracy (SD, %)
commercial H_2O_2 formulation (3%, v/v)	0.10	0.12 ± 0.03	+18
tap water	0.02	0.021 ± 0.004	+7
	0.10	0.085 ± 0.019	−15

Real Sample Analysis and Stability Studies. Tap water samples were also analyzed to assess the suitability of the sensor to detect hydrogen peroxide deriving from disinfection treatments of water.[42−44] In this context, tap water was first analyzed and spiked samples were obtained. The aqueous samples were spiked at 2 different levels, ∼LOQ and ∼5LOQ, to study the suitability of the developed sensor in real sample analysis. Table 2 shows the recoveries, expressed as average from 3 different replicates together with SD, compared to the theoretical (spiked amount). These results support the convenience of the proposed method for the analysis of low levels of H_2O_2 with no need for sample pretreatment steps. Storage stability studies were also performed (Figure 4B) with the papers, which are intended as ready-to-use sensing papers, stored at different conditions (4 and 28 °C) for different periods (from 0 to 30 days). As observed, the sensor maintained almost unaltered initial catalytic activity (>75%) for up to 7 days after its assembly, whatever the storage temperature. This allows the possible manufacturing and shipping to low-resource places for on-site analysis. However, only the sensor kept at 28 °C was able to produce a CL signal of 80% compared to the CL signal from day 0 when the time was extended to 14 days, giving 54% of the CL signal for the 4 °C sensor. This fact could be explained by the agglomeration of MOF at low temperatures, which decreases the mimetic activity of the PB-NPs@MIL-101(Fe). Additionally, SEM micrographs were

performed at times 0 and 14 d to check if either the composite was degraded or the structure was altered. As observed in Figure S12, the structure remains unaltered, which further confirms the obtained experimental results. For longer storage periods, 37% of the initial activity was observed when the sensor was stored for up to 30 days at 28 °C. The PB-NPs@MIL-101(Fe) composite has been used for obtaining a sensing paper for H_2O_2 rapid and sensitive detection. The proposed method has been compared to other recently reported methods for the determination of H_2O_2 (Table S1). Regarding the K_m H_2O_2 value, the developed sensor presents a better or similar value (10^{-8} to 10^{-9} M) to that reported in the literature,[17,45] which is markedly lower than others.[46–48] Besides, the V_{max} obtained for this methodology is comparable to that obtained using the MOF(Co) material[49] and much higher than the other examples. In terms of linearity, our protocol indeed presents a narrow range (1−2 orders of magnitude), whereas most of the other authors report 2−8 orders of magnitude.[50,51] This limitation can be easily overcome by simply diluting the sample. Finally, the reported LOD is one of the lowest (8.2×10^{-11} mol), only outperformed by the methods reported by Jia et al. (8×10^{-12} mol), Wu et al. (2.5×10^{-13} mol), and Nemati et al. (5.6×10^{-15} mol).[50–52] It is also noticeable that it is the first time that PB-NPs@MOF has been used to develop a sensing paper, and all the other approaches are in liquid format, with scarce potential for future implementation in portable analytical devices. Furthermore, the required amount of sample is as small as 10 μL, which could be convenient for clinical samples. Other important aspects of this method are as follows: the simplicity of the synthesis (drop-casting approach), the portability, and the cost-efficiency of a batch of sensors (n = 10, 1.5 euro) lead to this method becoming a promising alternative not only for screening purposes of H_2O_2 but also to design new approaches using MOF-based materials. A few H_2O_2 paper sensors have been developed, such as a colorimetric paper sensor based on other nanocomposites

such as Pd−Pt nanoparticles, hemin functionalized reduced graphene oxide (hemin-rGO) and carboxylated CNTs,[53] and a paper-based electrochemical sensor using PB as the electrochemical mediator,[54] the latter having the required sensitivity and ability to monitor H_2O_2 in aerosol but still requiring a smartphone-driven potentiostat. Other examples rely on the use of hydrogels, which undergo a reactive process and decompose in the presence of H_2O_2;[55] however, they require assay steps and incubation times, which hamper their actual portability (e.g., sequential incubations at different temperatures followed by recovery of the aqueous solution for absorbance measurements with a UV−vis spectrophotometer). Another work relies on fluorescence measurements of a microfluidic paper chip; however, the sustainability of the process is very low since it requires organic solvents and nongreen procedures, such as heating for 3 h at 160 °C.[56] Instead, our paper sensing platform, to the best of our knowledge, is the only add-and-measure paper sensor mimicking peroxidase activity. All the reagents required for the analysis are already integrated in the paper sensor, thus providing a novel approach for stand-alone CL paper sensors.

4. Conclusions

For the first time, we have explored the in situ growth of PBNPs onto the MIL-101(Fe) structure for the assembly of a sensing paper. The CL signal emission produced by the "nanozyme-on-paper" has been enhanced by the presence of this composite in the sensor compared to the individual components. Furthermore, PB-NPs@MIL-101(Fe) was fully characterized, suggesting that no morphological changes have occurred, although the synthesis has been performed on the paper surface. In this sense, several techniques, such as FT-IR, p-XRD, and TEM, have contrasted the presence of PB-NPs. After the careful optimization of the method, the sensor was successfully applied, as a proof of concept, to H2O2 determination in commercial hydrogen peroxide solutions and spiked tap water

samples. The method was able to detect as low as 8.2 μM (8.2×10^{-11} mol) with good accuracy (SD < 20%) and acceptable precision (RSD < 17%).[53–56] Despite these promising findings, further investigation will be performed to increase the linear range and to perform onfield analysis using portable detectors. In particular, despite the high signal intensity, which was suitable for smartphone-based detection (Figure 1), it will be necessary to extend the emission kinetics to enable implementation into a portable smartphone analytical platform. As strong points, the good storage stability (up to 14 days under atmospheric conditions) and the affordable price per sensor (0.15 euro) prompt the future applicability of this method for future sensing applications. For all of this, the MOF-based materials represent a good strategy to enhance the CL response and could serve as a guide for other researchers to use MOFs as host materials for different analytical challenges.

Author Contributions H.M.-P.-C.: conceptualization, methodology and design, formal analysis and investigation, writing-original draft M.M.C.: conceptualization, visualization, writing-review and editing E. M.: conceptualization, writing-review and editing, supervision, funding acquisition and resources.

Notes The authors declare no competing financial interest.

Acknowledgments

This research was in part funded by Project PRIN SMARTMASK4CF-code 2022XTCTWH-CUP J53D23007680006 funded by the Italian Ministry of University and Research and the Agritech National Research Center and received funding from the European Union Next-Generation EU National Recovery and Resilience Plan (NRRP), Mission 04 Component 2, investment 1.4-D.D. 1032 17/06/2022, CN00000022, and

investment 1.5-NextGenerationEU, call for tender no. 3277, dated 30/12/2021 and award number: 0001052, dated 23/06/2022. This work was also supported by projects PID2021-125459OB-I00 funded by MCIN/AEI/ 10.13039/501100011033, and by "ERDF A way of making Europe" by the European Union. The authors thank Dr. Giampaolo Lacarborara (Laboratory of Electrochemistry of Materials for Energetics of the Dept. of Chemistry "Giacomo Ciamician") for use of the field emission SEM and assistance in acquiring scanning electron micrographs.

References

(1) Wang, M.; Ma, J.; Guan, X.; Peng, W.; Fan, X.; Zhang, G.; Zhang, F.; Li, Y. J. Alloys Compd. 2019, 784, 827−833.

(2) Guo, S.; Wen, D.; Dong, S.; Wang, E. Talanta 2009, 77 (4), 1510−1517.

(3) Barnes, P. J. Antioxidants 2022, 11 (5), 965.

(4) Zhang, Z.; Lai, J.; Wu, K.; Huang, X.; Guo, S.; Zhang, L.; Liu, J. Talanta 2018, 180, 260−270.

(5) Giaretta, J. E.; Duan, H.; Oveissi, F.; Farajikhah, S.; Dehghani, F.; Naficy, S. ACS Appl. Mater. Interfaces 2022, 14 (18), 20491− 20505.

(6) Waris; Hasnat, A.; Hasan, S.; Bano, S.; Sultana, S.; Ibhadon, A. O.; Khan, M. Z. J. Mater. Chem. B 2023, 11 (29), 6762−6781.

(7) Nossol, E.; Zarbin, A. J. G. Adv. Funct. Mater. 2009, 19 (24), 3980−3986.

(8) Fiorito, P. A.; de Torresi, S. I. C. J. Electroanal. Chem. 2005, 581 (1), 31−37.

(9) Moscone, D.; D'Ottavi, D.; Compagnone, D.; Palleschi, G.; Amine, A. Anal. Chem. 2001, 73 (11), 2529−2535.

(10) Ricci, F.; Palleschi, G. Biosens. Bioelectron. 2005, 21 (3), 389− 407.

(11) Michopoulos, A.; Kouloumpis, A.; Gournis, D.; Prodromidis, M. I. Electrochim. Acta 2014, 146, 477−484.

(12) Su, L.; Xiong, Y.; Yang, H.; Zhang, P.; Ye, F. J. Mater. Chem. B 2016, 4 (1), 128−134.

(13) Yusuf, V. F.; Malek, N. I.; Kailasa, S. K. ACS Omega 2022, 7 (49), 44507−44531.

(14) Safaei, M.; Foroughi, M. M.; Ebrahimpoor, N.; Jahani, S.; Omidi, A.; Khatami, M. TrAC, Trends Anal. Chem. 2019, 118, 401− 425.

(15) Gu, Z.-Y.; Yang, C.-X.; Chang, N.; Yan, X.-P. Acc. Chem. Res. 2012, 45 (5), 734−745.

(16) Niu, X.; Li, X.; Lyu, Z.; Pan, J.; Ding, S.; Ruan, X.; Zhu, W.; Du, D.; Lin, Y. Chem. Commun. 2020, 56 (77), 11338−11353.

(17) Cui, F.; Deng, Q.; Sun, L. RSC Adv. 2015, 5 (119), 98215− 98221.

(18) Su, L.; Xiong, Y.; Yang, H.; Zhang, P.; Ye, F. J. Mater. Chem. B 2016, 4 (1), 128−134.

(19) Tong, L.; Wu, L.; Zai, Y.; Zhang, Y.; Su, E.; Gu, N. Biosens. Bioelectron. 2023, 219, 114787. (20) Pérez-Cejuela, H. M.; Carrasco-Correa, E. J.; Shahat, A.; SimóAlfonso, E. F.; Herrero-Martínez, J. M. J. Sep. Sci. 2019, 42 (4), 834− 842.

(21) Cui, F.; Deng, Q.; Sun, L. RSC Adv. 2015, 5 (119), 98215− 98221.

(22) Huang, J.; Pan, J.; Song, Y.; Lin, Q.; Xu, Y.; Dai, Z.; Liu, S.-Y. TrAC, Trends Anal. Chem. 2024, 173, 117619.

(23) Xing, Y.; Si, H.; Sun, D.; Hou, X. Microchem. J. 2020, 156, 104929.

(24) Skobelev, I. Y.; Sorokin, A. B.; Kovalenko, K. A.; Fedin, V. P.; Kholdeeva, O. A. J. Catal. 2013, 298, 61−69.

(25) Zhu, Q.; Chen, Y.; Wang, W.; Zhang, H.; Ren, C.; Chen, H.; Chen, X. Sens. Actuators, B 2015, 210, 500−507.

(26) Li, D.; Zhang, S.; Feng, X.; Yang, H.; Nie, F.; Zhang, W. Sens. Actuators, B 2019, 296, 126631. (27) Gumus, I.; Karatas¸, Y.; Gülcan, M. Catal. Sci. Technol. 2020, 10 (15), 4990−4999.

(28) Hu, Z.; Wu, H.; Zhu, F.; Komarneni, S.; Ma, J. Inorg. Chem. Commun. 2022, 144, 109902.

(29) Li, W.-P.; Su, C.-H.; Tsao, L.-C.; Chang, C.-T.; Hsu, Y.-P.; Yeh, C.-S. ACS Nano 2016, 10 (12), 11027−11036.

(30) Li, W.-P.; Su, C.-H.; Tsao, L.-C.; Chang, C.-T.; Hsu, Y.-P.; Yeh, C.-S. ACS Nano 2016, 10 (12), 11027−11036.

(31) Yan, D.; Hu, H.; Gao, N.; Ye, J.; Ou, H. Appl. Surf. Sci. 2019, 498, 143836.

(32) Liu, Y.; Xie, Y.; Dai, M.; Gong, Q.; Dang, Z. Materials 2019, 12 (9), 1453.

(33) Wu, Y.; Liu, Z.; Bakhtari, M. F.; Luo, J. Environ. Sci. Pollut. Res. 2021, 28 (37), 51391−51403. (34) Martínez-Pérez-Cejuela, H.; Calabretta, M.; Bocci, V.; D'Elia, M.; Michelini, E. Biosensors 2023, 13 (4), 451.

(35) Lopreside, A.; Montali, L.; Wang, B.; Tassoni, A.; Ferri, M.; Calabretta, M. M.; Michelini, E. Biosens. Bioelectron. 2021, 194, 113569.

(36) Bi, X.; Zhao, L.-X.; Xie, M.; Zhang, C.; Lin, J.-M.; Zhao, R.-S. Chem. Eng. J. 2022, 445, 136751. (37) Ranjan, R.; Esimbekova, E. N.; Kirillova, M. A.; Kratasyuk, V. A. Anal. Chim. Acta 2017, 971, 1−13.

(38) Wang, Y.; Wang, S.; Huang, M.; Chen, F. Microchem. J. 2020, 158, 105213.

(39) Li, S.; Zhang, Y.; Qiao, S.; Zhou, J. J. Water Proc. Eng. 2023, 53, 103821.

(40) Boczkaj, G.; Fernandes, A. Chem. Eng. J. 2017, 320, 608−633.

(41) Hu, H.; Zhang, H.; Chen, Y.; Ou, H. Environ. Sci. Pollut. Res. 2019, 26 (24), 24720−24732.

(42) Zhao, Z.; Pan, S.; Ye, Y.; Zhang, X.; Pan, B. Chem. Eng. J. 2020, 381, 122667.

(43) Ye, Y.; Shan, C.; Zhang, X.; Liu, H.; Wang, D.; Lv, L.; Pan, B. Environ. Sci. Technol. 2018, 52 (18), 10657−10664.

(44) Yang, B.; Cheng, X.; Zhang, Y.; Li, W.; Wang, J.; Tian, Z.; Du, E.; Guo, H. J. Hazard. Mater. 2021, 407, 124853.

(45) Ai, L.; Li, L.; Zhang, C.; Fu, J.; Jiang, J. Chem. Eur. J. 2013, 19 (45), 15105−15108.

(46) Qin, F.-X.; Jia, S.-Y.; Wang, F.-F.; Wu, S.-H.; Song, J.; Liu, Y. Catal. Sci. Technol. 2013, 3 (10), 2761.

(47) Gao, L.; Zhuang, J.; Nie, L.; Zhang, J.; Zhang, Y.; Gu, N.; Wang, T.; Feng, J.; Yang, D.; Perrett, S.; Yan, X. Nat. Nanotechnol. 2007, 2 (9), 577−583.

(48) Mu, J.; Wang, Y.; Zhao, M.; Zhang, L. Chem. Commun. 2012, 48 (19), 2540.

(49) Li, D.; Zhang, S.; Feng, X.; Yang, H.; Nie, F.; Zhang, W. Sens. Actuators, B 2019, 296, 126631. (50) Jia, Y.; Sun, S.; Cui, X.; Wang, X.; Yang, L. Talanta 2019, 205, 120139.

(51) Wu, Y.; Wang, J.; Cui, H. Anal. Bioanal. Chem. 2022, 414 (1), 367−375.

(52) Nemati, A.; Chaichi, M. J.; Lakouraj, M. M.; Hosseinkhani, S.; Seyedalipour, B. J. Photochem. Photobiol., A 2023, 437, 114332.

(53) Li, Y.; Zhang, X.; Shen, J.; Qi, W. ChemNanoMat 2023, 9 (5), No. e202200569.

(54) Fiore, L.; Mazzaracchio, V.; Galloni, P.; Sabuzi, F.; Pezzola, S.; Matteucci, G.; Moscone, D.; Arduini, F. Microchem. J. 2021, 166, 106249.

(55) Li, R.; Cheng, R.; Liu, J.; Bi, Y.; Song, P.; Hu, Q.; Yu, L. Talanta 2024, 276, 126244.

(56) Yu, L.; He, C.; Zheng, Q.; Feng, L.; Xiong, L.; Xiao, Y. J. Mater. Chem. C 2020, 8 (10), 3562−3570.

SUPPORTING INFORMATION

Chemiluminescence "add-and-measure" sensing paper based on Prussian Blue/Metal-Organic Framework MIL-101 nanozyme for rapid hydrogen peroxide detection

*Héctor Martínez-Pérez-Cejuela[‡], Maria Maddalena Calabretta[†], Elisa Michelini[†,¥,]**

[‡] Department of Analytical Chemistry, University of Valencia, Dr. Moliner 50, 46100, Burjassot, Valencia, Spain; [†]Department of Chemistry "Giacomo Ciamician", University of Bologna, Via P. Gobetti 85, 40129, Bologna, Italy; [¥] IRCCS Azienda Ospedaliero-Universitaria di Bologna, 40138 Bologna, Italy

Table of contents

EXPERIMENTAL SECTION

Synthesis of MIL-101(Cr): 5 mmol of metal precursor ($Cr(NO_3)_3 \cdot 9H_2O$) was weighed and mixed with 2 mmol of terephthalic acid (TA) in 15 mL of MQ-water. The molar ratio was set at 1:2.5:417 for TA:Cr(III):H_2O. The mixtures were homogenized and introduced in a Teflon-lined stainless steel autoclave. After its sealing, the mixture was heated up to 150 ºC for 12 h. Then, the resulting green powder was collected by centrifugation at 14,000 g for 10 min and washed with DMF several times (3 x 10 mL). Finally, further purification was performed as indicated for MIL-101(Fe) in Section 2.4. with methanol at 60 ºC and drying process.

Synthesis of MIL-101(Al): 2 mmol of $AlCl_3 \cdot 6H_2O$ and 3 mmol of terephthalic acid were solved in 40 mL of DMF. The molar ratio was set at 1:1.5:258 for Al(III):TA:DMF. The mixture was homogenized in the ultrasonic bath for 30 min and placed in a Teflon-lined stainless steel autoclave. The synthesis was performed for 72 h at 130 ºC. The resulting palish yellow was centrifuged (14,000 g for 10 min) and washed with DMF several times (3 x 20 mL). Finally, further purification was performed as indicated for MIL-101(Fe) in the Section 2.4. with methanol at 60 ºC and drying process.

Synthesis of bare PB-NPs: 1.1 mmol of citric acid was added to a previously prepared solution of 1 mM $FeCl_3 \cdot 6H_2O$ (40 mL). The mixture was homogenized and heated up to 60 ºC. Then, 40 mL of 1 mM $K_4Fe(CN)_6 \cdot 3H_2O$ were added dropwise for 30 min at 60 ºC under vigorous stirring. After the addition of this latter reagent, an intensive blue color appeared with a perfect dispersion of NPs. The resulting PB-NPs were naturally cooled to room temperature under mild stirring for approximately 1 h.

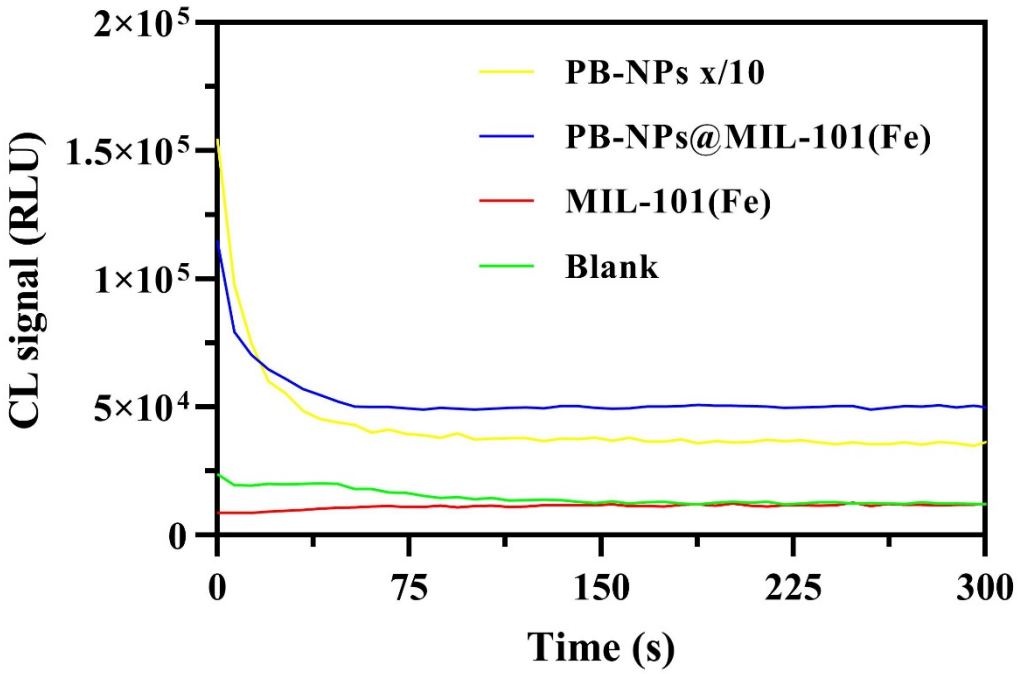

Figure S1. Preliminary studies in batch using 384-well plate comparing MOF(Fe), composite, and pristine PB-NPs. Experimental conditions: 5.0 µL PB-NPs@MIL-101 dispersions (500 mg L^{-1}), 5.0 µL of luminol 0.025 M (pH 12.0) and 10.0 µL of 0.1 mM H_2O_2.

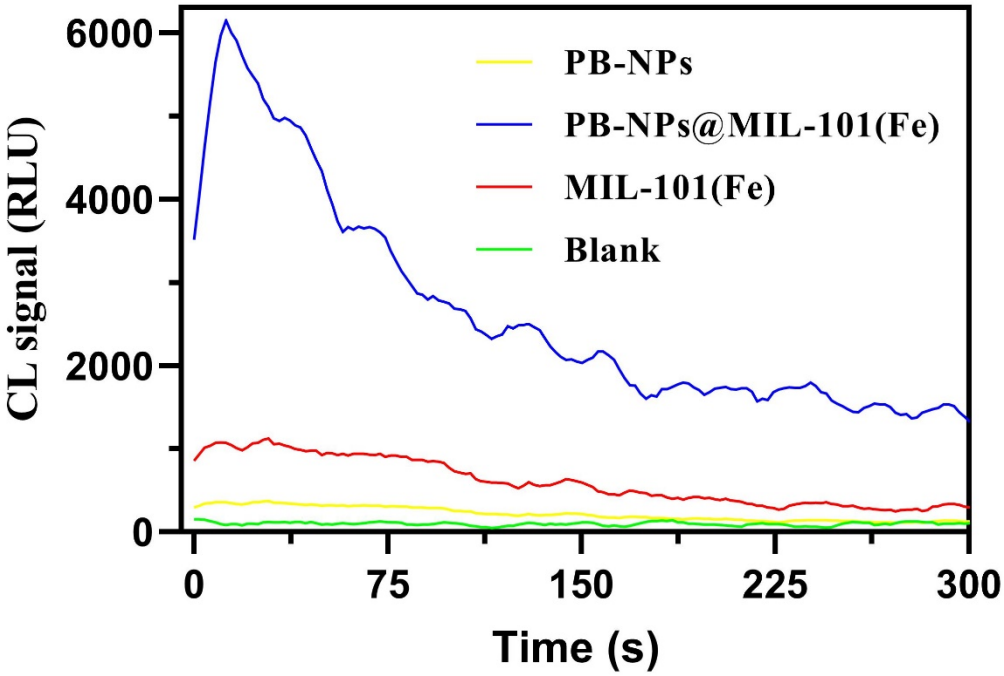

Figure S2. Preliminary chemiluminescence studies in paper-sensor comparing MOF(Fe), composite, and pristine PB-NPs. Experimental conditions: dried 10 µL commercial luminol and 10 µL of 2000 mg L^{-1} PB-NPs@MIL-101(Fe) (or bare MIL-101(Fe) or PB-NPs) and 10 µL of H_2O_2 0.1 mM.

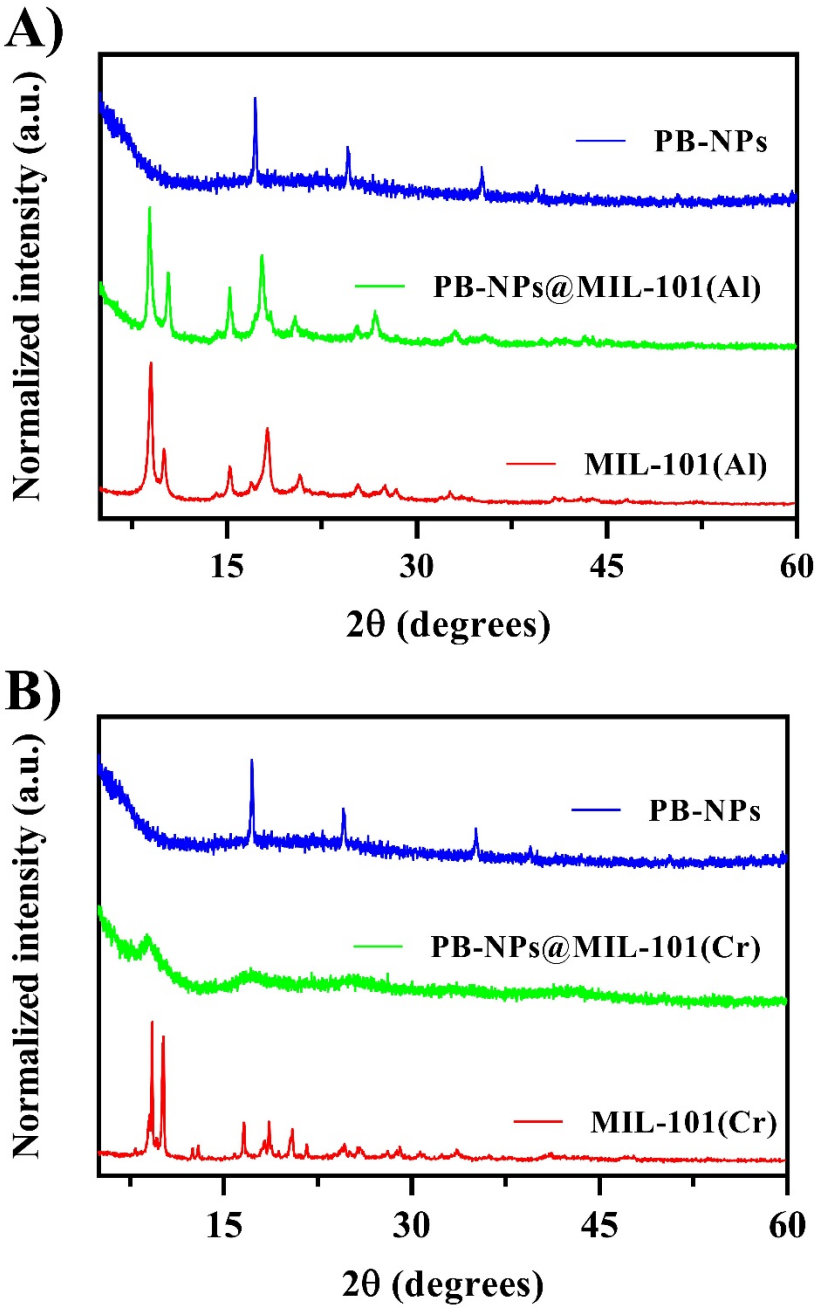

Figure S3. p-XRD spectra from 5 to 60 degree (2Θ) for MIL-101(Cr, Al), bare PB-NPs, and their respective composites.

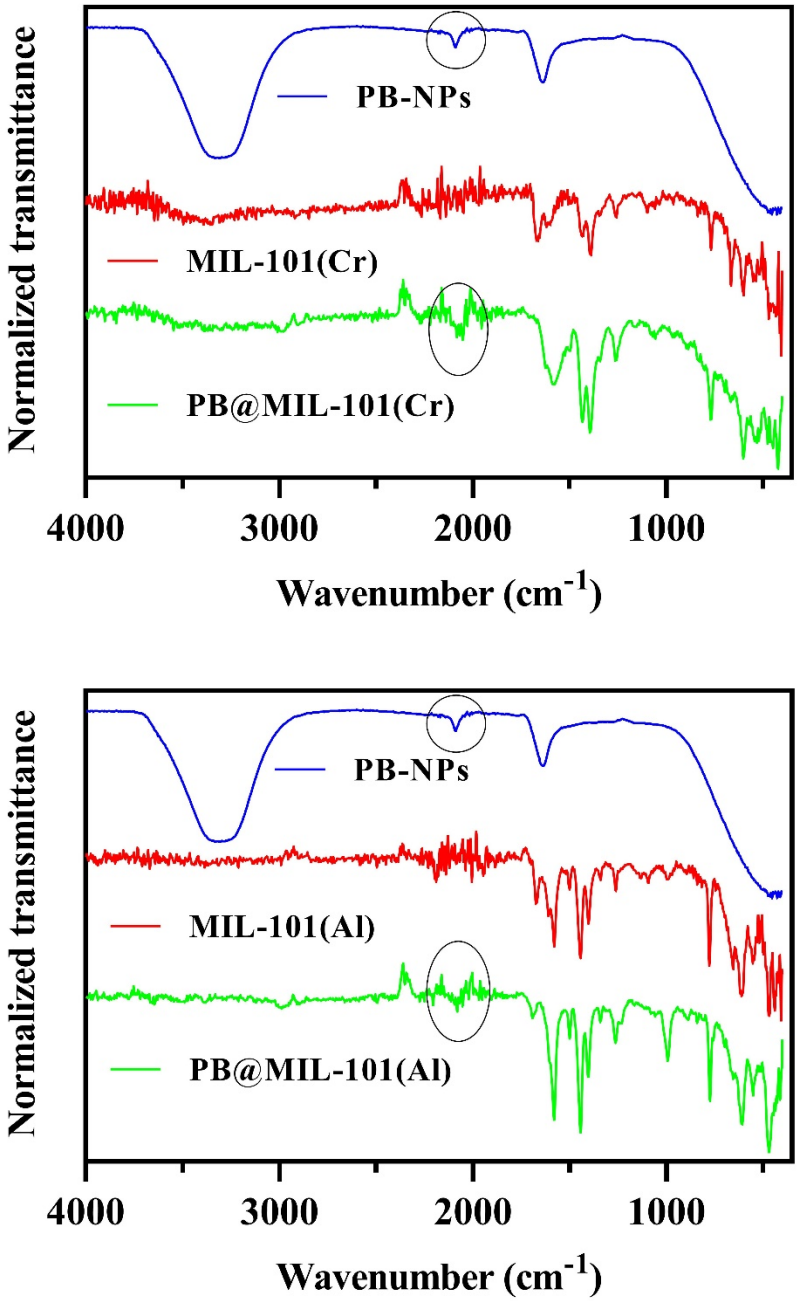

Figure S4. FT-IR spectra from 4000 to 400 cm^{-1} for MIL-101(Cr, Al), bare PB-NPs, and their respective composites.

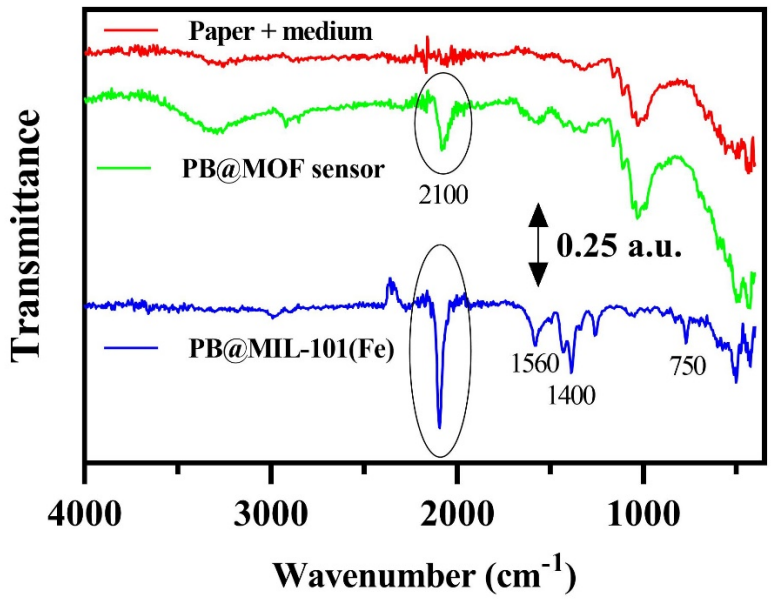

Figure S5. FT-IR spectra from 4000 to 400 cm^{-1} for different sensors and bulk composite.

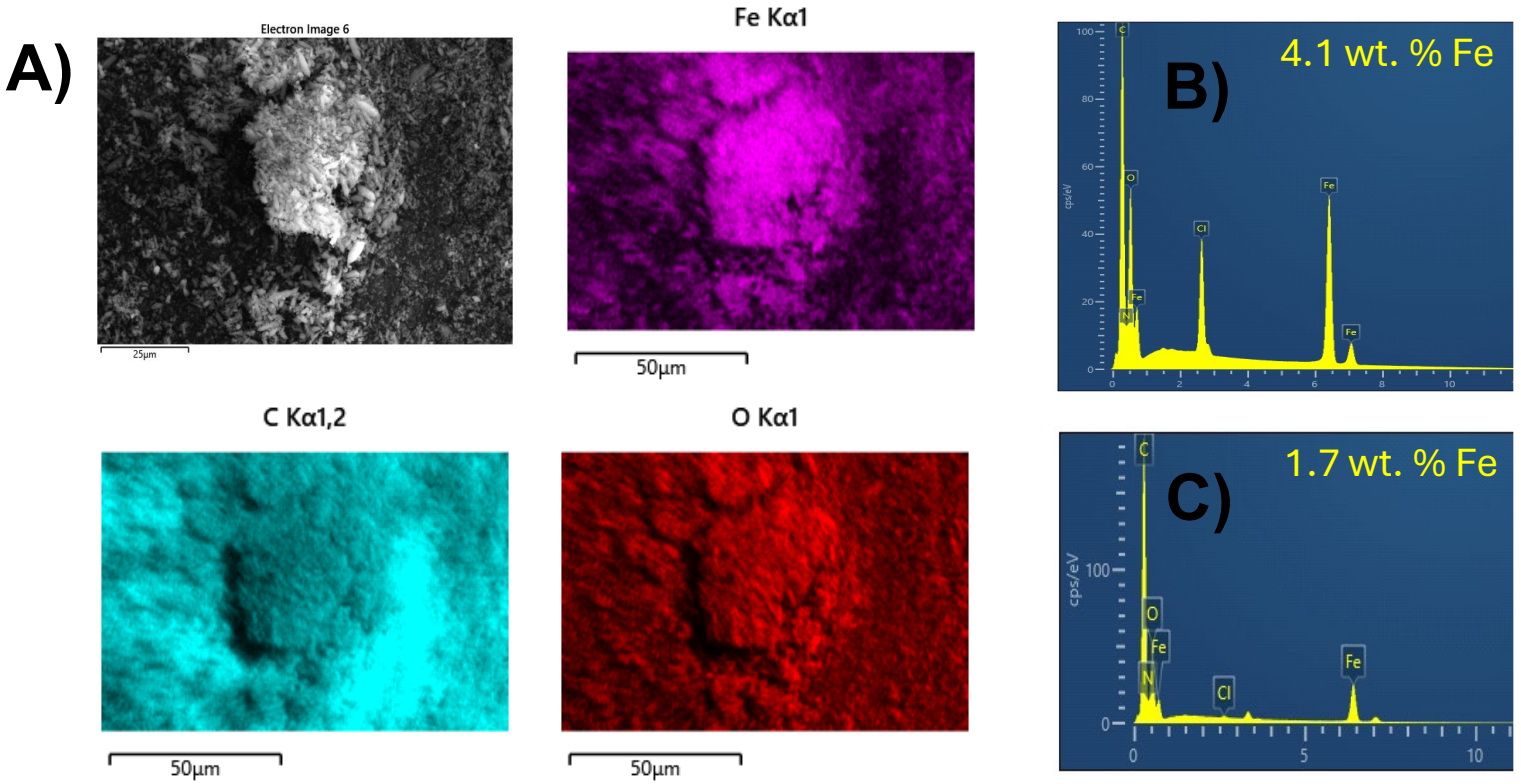

Figure S6. A) Mapping and B) EDX analysis of the PB-NPs@MIL-101(Fe) and C) EDX analysis of MIL-101(Fe).

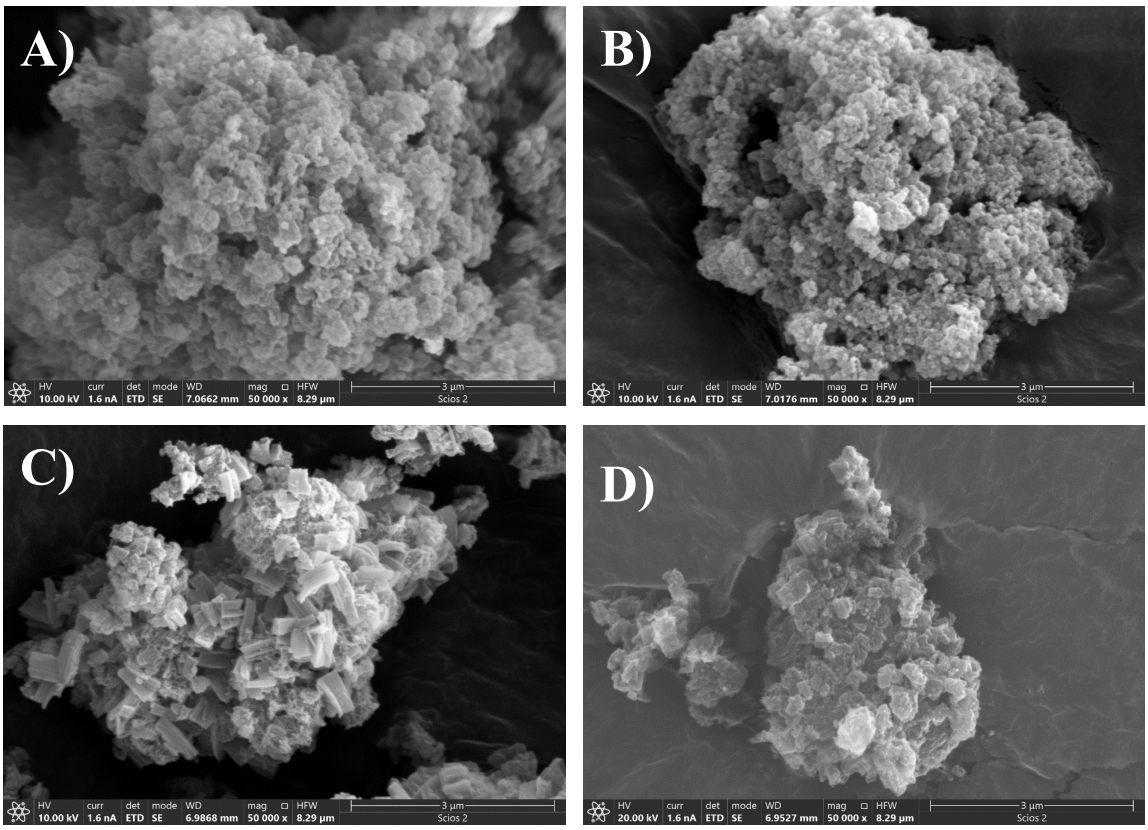

Figure S7. SEM micrographs of A) MIL-101(Cr); B) PB-NPs@MIL-101(Cr); C) MIL-101(Al); D) PB-NPs@MIL-101(Al). Magnification and scale-bars are included in their respective images.

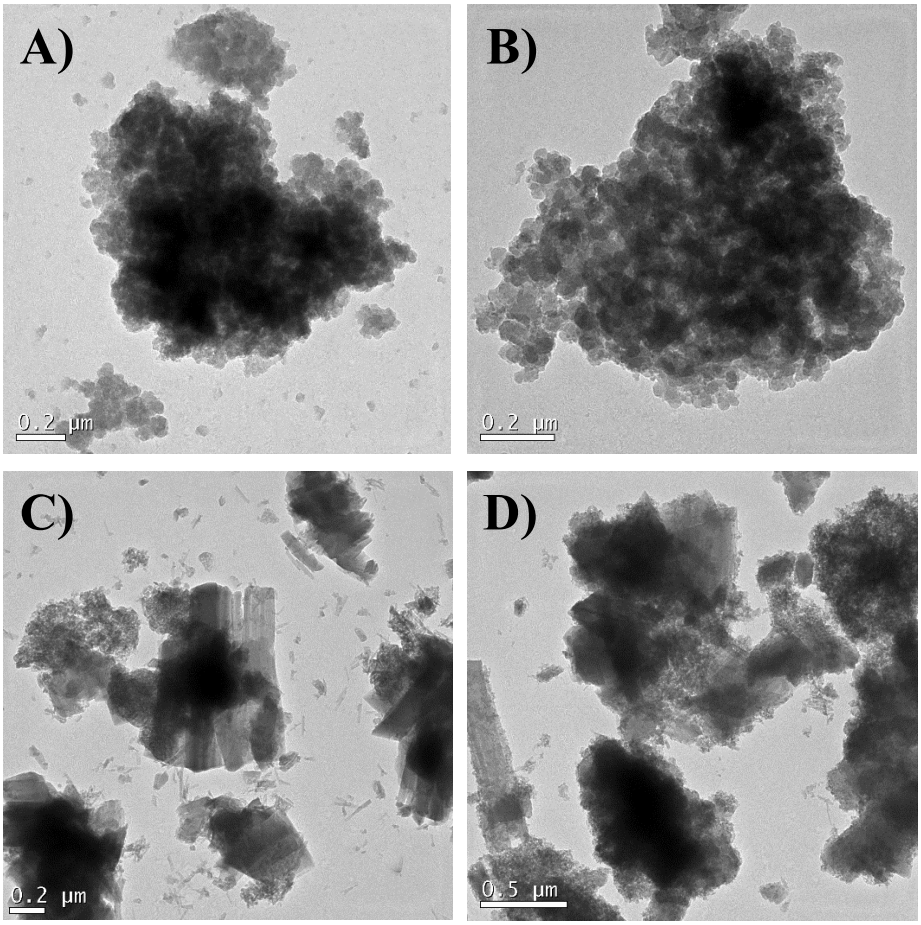

Figure S8. TEM micrographs of A) MIL-101(Cr); B) PB-NPs@MIL-101(Cr); C) MIL-101(Al); D) PB-NPs@MIL-101(Al). Scale-bars are included in their respective images.

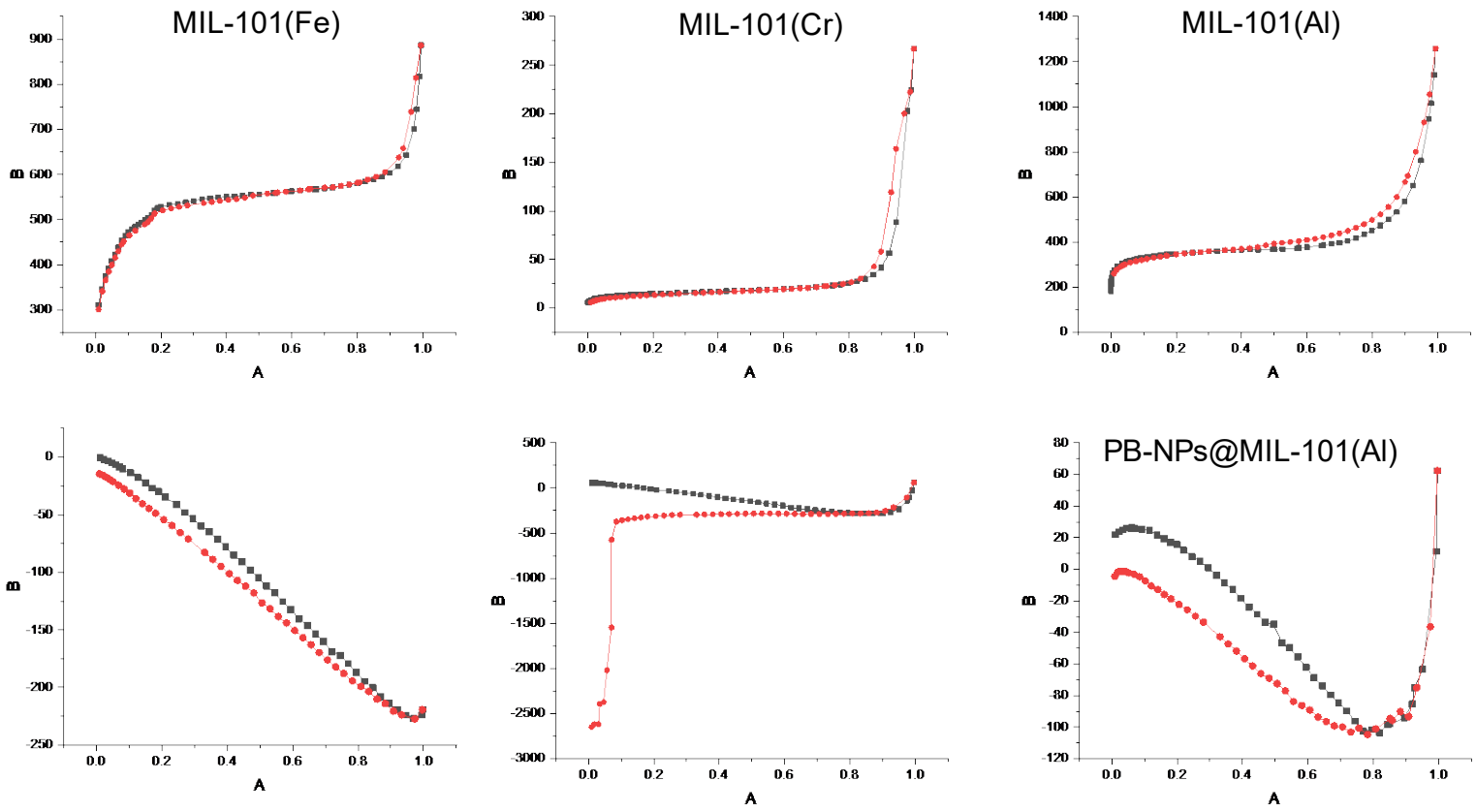

Figure S9. N_2 (77 K) adsorption/desorption isotherms before and after PB-NPs impregnation. Black and red lines indicate the adsorption and desorption isotherms, respectively (A: Relative pressure (P/P_0); and B: Vol. Adsorbed ($cm^3\ g^{-1}$)

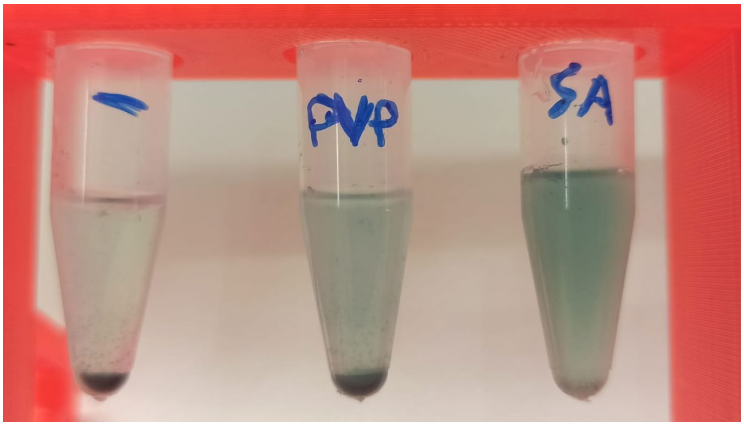

Figure S10. Different dispersions of 500 µg of PB-NPs@MIL-101(Fe) using 1% (w/v) of PVP and SA in Tris-HCl 50 mM (pH 7.8) after their incubation without stirring for 2 h.

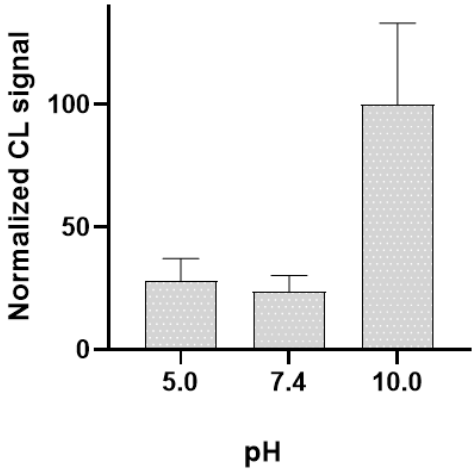

Figure S11. pH stability study. Stability studies at different pH were performed by analyzing H_2O_2 (0.1 mM) with the PB-NPs@MIL-101(Fe) sensing paper in 50 mM Tris-HCl by adjusting the pH to 5.0, 7.4, and 10.0, respectively

.

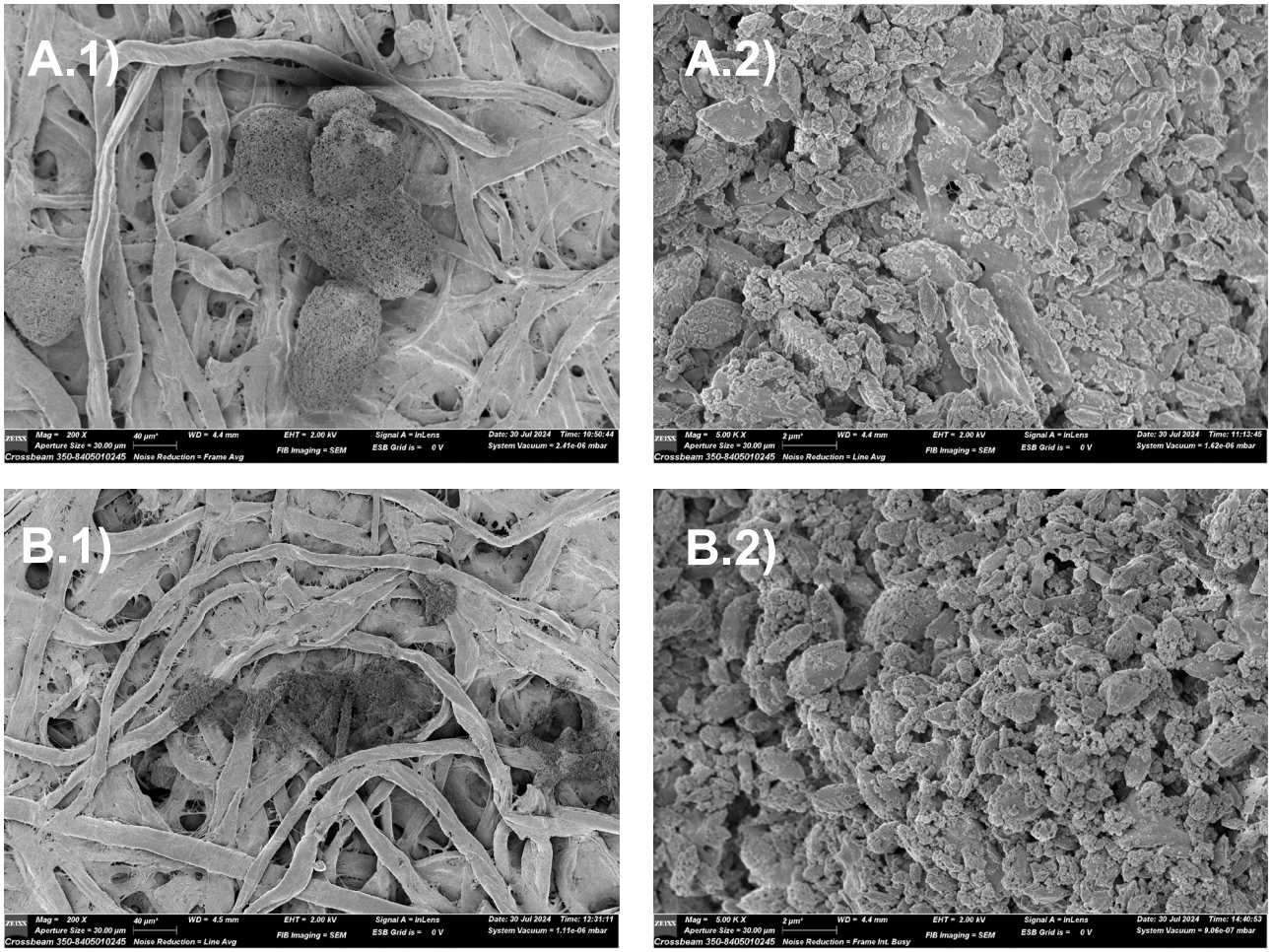

Figure S12. SEM micrographs of PB-NPs@MIL-101(Fe) at days A) 0 and B) 14. Magnification (1-2) and scale-bars are included in their respective images.

Table S1. Comparison of the nanozyme sensing paper with other reported methods for H_2O_2 detection.

Material	Km H_2O_2 (mol)	(Co)Substrate	Reaction volume	V_{max} (Mol s^{-1})	LDR (mol)	LOD_{H2O2} (mol)	Ref.
Co_3O_4	$4.7 \cdot 10^{-5}$	TMB/H_2O_2	3000 µL	$3.63 \cdot 10^{-10}$	$1.67 \cdot 10^{-8}$ – $8.33 \cdot 10^{-6}$	$3.33 \cdot 10^{-8}$	1
Fe_3O_4	$2.03 \cdot 10^{-4}$	TMB/H_2O_2	1316 µL	$1.29 \cdot 10^{-10}$	-	-	2
MWCNT	$2.66 \cdot 10^{-7}$	TMB/H_2O_2	200 µL	$2.22 \cdot 10^{-11}$	$2 \cdot 10^{-10}$ – $3 \cdot 10^{-7}$	$2 \cdot 10^{-11}$	3
PB	$1.54 \cdot 10^{-6}$	TMB/H_2O_2	200 µL	$8.38 \cdot 10^{-13}$	-	-	3
PB	$7.82 \cdot 10^{-6}$	TMB/H_2O_2	1000 µL	$2.4 \cdot 10^{-11}$	-	-	4
HRP	$4.87 \cdot 10^{-6}$	TMB/H_2O_2	1316 µL	$1.15 \cdot 10^{-10}$	-	-	2
Hemin@MOF	$1.64 \cdot 10^{-5}$	TMB/H_2O_2	1500 µL	$1.35 \cdot 10^{-10}$	$7.5 \cdot 10^{-9}$ – $3 \cdot 10^{-7}$	-	5
MIL-53(Fe)	$4.2 \cdot 10^{-8}$	TMB/H_2O_2	1050 µL	$1.95 \cdot 10^{-11}$	$9.98 \cdot 10^{-10}$ – $2.00 \cdot 10^{-8}$	$1.37 \cdot 10^{-10}$	6
MIL-101(Cr)	$1.06 \cdot 10^{-6}$	TMB/H_2O_2	1000 µL	$9.7 \cdot 10^{-11}$	-	-	4
MIL-101(Fe)	$5.80 \cdot 10^{-9}$	TMB/H_2O_2	100 µL	$2.22 \cdot 10^{-12}$	$2.40 \cdot 10^{-6}$ – $1 \cdot 10^{-8}$	$1.5 \cdot 10^{-11}$	7
MOF(Ce)	-	TMB/H_2O_2	300 µL	-	$1.2 \cdot 10^{-6}$ – $4.8 \cdot 10^{-6}$	$3 \cdot 10^{-9}$	8
Fe_3O_4	-	ABTS/H_2O_2	1000 µL	-	$5 \cdot 10^{-9}$ – $1 \cdot 10^{-7}$	$3.00 \cdot 10^{-9}$	9
MIL-101(Cr)	-	Luciferin/H_2O_2	200 µL	-	$2 \cdot 10^{-6}$ – $2 \cdot 10^{-14}$	$5.6 \cdot 10^{-15}$	10
ABEI/$CuFe_2O_4$	-	ABEI/H_2O_2	100 µL	-	$1 \cdot 10^{-12}$ – $1 \cdot 10^{-8}$	$2.5 \cdot 10^{-13}$	11
POMs	-	Luminol/H_2O_2	1600 µL	-	$2.67 \cdot 10^{-11}$ – $8 \cdot 10^{-9}$	$8 \cdot 10^{-12}$	12
MOF(Co)[a]	$1.55 \cdot 10^{-5}$	Luminol/H_2O_2	4000 µL	$1.29 \cdot 10^{-5}$	$6 \cdot 10^{-12}$ – $5 \cdot 10^{-9}$	-	13
MIL-101(Cr)	-	Luminol/H_2O_2	310 µL	-	$9.3 \cdot 10^{-10}$ – $3.1 \cdot 10^{-8}$	$1.55 \cdot 10^{-10}$	14
MIL-101(Fe)	$3.82 \cdot 10^{-9}$	Luminol/H_2O_2	10 µL (45 µL)	$3.65 \cdot 10^{-5}$	$1 \cdot 10^{-11}$ – $5 \cdot 10^{-10}$	(8.2 µM) $8.2 \cdot 10^{-11}$	This work

Abbreviations: MWCNT: Multi-Walled Carbon Nanotube ; TMB: 3,3′,5,5′-Tetramethylbenzidine; ABTS: 2,2‘-azino-bis(3-ethylbenzo-thiazoline-6-sulfonic acid) diammonium salt; ABEI: N-(4-aminobutyl)-N-ethylisoluminol; POM: olyoxometalates; LDR: linear dynamic range; LOD: limit of detection.

[a]The Km and the V_{max} was calculated with TMB/H_2O_2 system

References

(1) Mu, J.; Wang, Y.; Zhao, M.; Zhang, L. Intrinsic Peroxidase-like Activity and Catalase-like Activity of Co3O4 Nanoparticles. *Chemical Communications* **2012**, *48* (19), 2540. https://doi.org/10.1039/c2cc17013b.

(2) Gao, L.; Zhuang, J.; Nie, L.; Zhang, J.; Zhang, Y.; Gu, N.; Wang, T.; Feng, J.; Yang, D.; Perrett, S.; Yan, X. Intrinsic Peroxidase-like Activity of Ferromagnetic Nanoparticles. *Nat Nanotechnol* **2007**, *2* (9), 577–583. https://doi.org/10.1038/nnano.2007.260.

(3) Wang, T.; Fu, Y.; Chai, L.; Chao, L.; Bu, L.; Meng, Y.; Chen, C.; Ma, M.; Xie, Q.; Yao, S. Filling Carbon Nanotubes with Prussian Blue Nanoparticles of High Peroxidase-Like Catalytic Activity for Colorimetric Chemo- and Biosensing. *Chemistry – A European Journal* **2014**, *20* (9), 2623–2630. https://doi.org/10.1002/chem.201304035.

(4) Su, L.; Xiong, Y.; Yang, H.; Zhang, P.; Ye, F. Prussian Blue Nanoparticles Encapsulated inside a Metal–Organic Framework via in Situ Growth as Promising Peroxidase Mimetics for Enzyme Inhibitor Screening. *J Mater Chem B* **2016**, *4* (1), 128–134. https://doi.org/10.1039/C5TB01924A.

(5) Qin, F.-X.; Jia, S.-Y.; Wang, F.-F.; Wu, S.-H.; Song, J.; Liu, Y. Hemin@metal–Organic Framework with Peroxidase-like Activity and Its Application to Glucose Detection. *Catal Sci Technol* **2013**, *3* (10), 2761. https://doi.org/10.1039/c3cy00268c.

(6) Ai, L.; Li, L.; Zhang, C.; Fu, J.; Jiang, J. MIL-53(Fe): A Metal–Organic Framework with Intrinsic Peroxidase-Like Catalytic Activity for Colorimetric Biosensing. *Chemistry – A European Journal* **2013**, *19* (45), 15105–15108. https://doi.org/10.1002/chem.201303051.

(7) Cui, F.; Deng, Q.; Sun, L. Prussian Blue Modified Metal–Organic Framework MIL-101(Fe) with Intrinsic Peroxidase-like Catalytic Activity as a Colorimetric Biosensing Platform. *RSC Adv* **2015**, *5* (119), 98215–98221. https://doi.org/10.1039/C5RA18589K.

(8) Wei, X.; Li, Y.; Qi, S.; Chen, Y.; Yin, M.; Zhang, L.; Tian, X.; Gong, S.; Wang, F.; Zhu, Y.; Liu, Y.; Qiu, J.; Xu, D. Ce-MOF Nanosphere as Colorimetric Sensor with High Oxidase Mimicking Activity for Sensitive Detection of H2O2. *J Inorg Organomet Polym Mater* **2022**, *32* (9), 3595–3600. https://doi.org/10.1007/s10904-022-02422-w.

(9) Wei, H.; Wang, E. Fe_3O_4 Magnetic Nanoparticles as Peroxidase Mimetics and Their Applications in H_2O_2 and Glucose Detection. *Anal Chem* **2008**, *80* (6), 2250–2254. https://doi.org/10.1021/ac702203f.

(10) Nemati, A.; Chaichi, M. J.; Lakouraj, M. M.; Hosseinkhani, S.; Seyedalipour, B. A Bioluminescent Earthworm Luciferase Mimetic MIL-101(Cr)-MOF for Enhanced Luciferin Chemiluminescence and H2O2 Sensing. *J Photochem Photobiol A Chem* **2023**, *437*, 114332. https://doi.org/10.1016/j.jphotochem.2022.114332.

(11) Wu, Y.; Wang, J.; Cui, H. Chemiluminescent Magnetic Nanoparticles with Good Catalytic Activity and Rapid Separation Capability and Sensitive Sensing for H2O2. *Anal Bioanal Chem* **2022**, *414* (1), 367–375. https://doi.org/10.1007/s00216-021-03597-w.

(12) Jia, Y.; Sun, S.; Cui, X.; Wang, X.; Yang, L. Enzyme-like Catalysis of Polyoxometalates for Chemiluminescence: Application in Ultrasensitive Detection of H2O2 and Blood Glucose. *Talanta* **2019**, *205*, 120139. https://doi.org/10.1016/j.talanta.2019.120139.

(13) Li, D.; Zhang, S.; Feng, X.; Yang, H.; Nie, F.; Zhang, W. A Novel Peroxidase Mimetic Co-MOF Enhanced Luminol Chemiluminescence and Its Application in Glucose Sensing. *Sens Actuators B Chem* **2019**, *296*, 126631. https://doi.org/10.1016/j.snb.2019.126631.

(14) Yu, H.; Long, D. Highly Chemiluminescent Metal-Organic Framework of Type MIL-101(Cr) for Detection of Hydrogen Peroxide and Pyrophosphate Ions. *Microchimica Acta* **2016**, *183* (12), 3151–3157. https://doi.org/10.1007/s00604-016-1963-8.